

INVESTIGATION OF AERODYNAMIC FORCES ON NACA AIRFOILS



UNIVERSITI TEKNIKAL MALAYSIA MELAKA

INVESTIGATION OF AERODYNAMIC FORCES ON NACA AIRFOILS

EMANNUEL CHAI



A report submitted

In fulfillment of the requirement for the degree of
Bachelor of Mechanical Engineering

UNIVERSITI TEKNIKAL MALAYSIA MELAKA

2019

DECLARATION

I declare that this project entitled “Investigation of Aerodynamic Forces on NACA Airfoils” is the result of my own work except as cited in the references.

Signature :

Name : Emmanuel Chai

Date :



اونيورسيتي تيكنيكل مليسيا ملاك

UNIVERSITI TEKNIKAL MALAYSIA MELAKA

APPROVAL

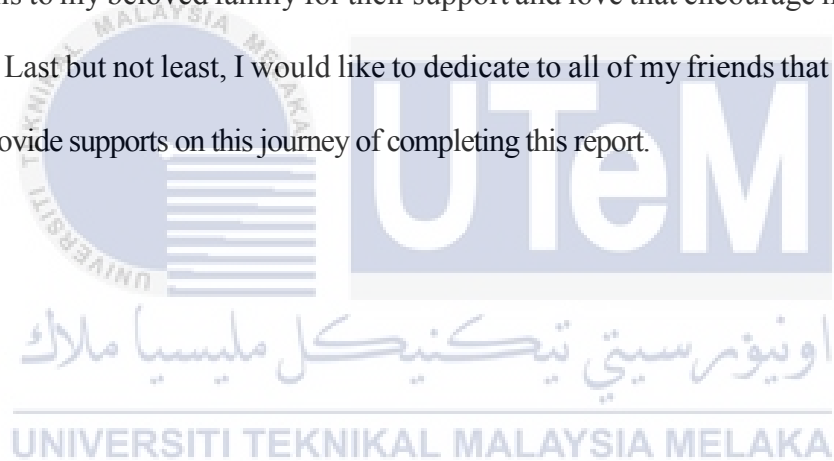
I hereby declare that I have read this project report and in my opinion this report is sufficient in terms of scope and quality for the award of the degree of Bachelor of Mechanical Engineering.

Signature :
Supervisor Name : En.Shamsul Bahari Bin Azraai
Date :



DEDICATION

This report is dedicated to En. Shamsul Bahari Bin Azraai for his guidance, inspiration and teaching that I was able to successfully completed it. I also would like to dedicated this to my beloved family for their support and love that encourage me on finishing this project. Last but not least, I would like to dedicate to all of my friends that lend me helping hands and provide supports on this journey of completing this report.



ABSTRACT

The aim of this project is to investigate the aerodynamic force on NACA airfoils by using Computational Fluid Dynamic simulation. ANSYS FLUENT 16 was used as the software for the CFD simulation of NACA 4412 and NACA 4418 in two different turbulence models which are Spalart-Allmaras (S-A) and Transition Shear Stress Transport (SST). The CFD simulation were done in three different air velocities of 10 m/s, 20 m/s and 30 m/s. The angle of attack of the airfoil also varied from 0° to 50° with increment of 5° . These two airfoils were chosen because both different maximum thickness but have the same mean camber line and maximum camber. The airfoil was designed in Solidworks with chord length of 100 mm. A rectangular domain of 300 mm x 300 mm x 450 mm was chosen as the fluid domain to mimic the experiment in wind tunnel with the same dimension of test section. The results for simulated aerodynamic forces between the two airfoils with two different turbulence models were analysed and discussed. Besides, results for the three different air velocity also analysed and the best angle of attack for the airfoils were determine. From the results, the stall angle for both NACA 4412 and NACA 4418 is at 45° for air velocity of 20 m/s and 30 m/s while the stall angle for both airfoils is 40° at 10 m/s. The effect of thickness of the airfoil on aerodynamic forces was also studied where NACA 4418 generate more lift force at its best angle of attack compare to NACA 4412. The performance for NACA 4418 is better than NACA 4412.

ABSTRAK

Tujuan projek ini dijalankan adalah untuk menyiasat daya aerodinamik pada aerofoil NACA dengan menggunakan simulasi "Computational Fluid Dynamic". ANSYS FLUENT 16 digunakan sebagai perisian untuk simulasi CFD pada NACA 4412 dan NACA 4418 dalam dua model pergolakan yang berbeza iaitu Spalart-Allmaras (S-A) dan Transition Shear Stress Transport (SST). Simulasi CFD dilakukan dalam tiga kelajuan udara yang berbeza iaitu 10 m/s, 20 m/s dan 30 m/s. Sudut serangan airfoil juga diubah dari 0 ° hingga 50° dengan kenaikan 5°. Kedua-dua airfoil ini dipilih kerana kedua-dua ketebalan maksimum yang berbeza tetapi mempunyai purata garis camber yang sama dan camber maksimum. Aerofoil ini direka bentuk dalam Solidworks dengan panjang kord 100mm. Domain segi empat tepat 300 mm x 300 mm x 450 mm dipilih sebagai domain bendalir untuk meniru percubaan ekperimentasi dalam terowong angin dengan dimensi yang sama pada bahagian ujian. Keputusan untuk daya aerodinamik yang disimulasi antara kedua-dua airfoil dengan dua model pergolakan yang berbeza dianalisis dan dibincangkan. Selain itu, keputusan untuk tiga halaju udara yang berbeza juga dianalisis dan sudut serangan yang terbaik untuk airfoil ditentukan pada setiap kelajuan. Hasil dari simulasi, sudut serangan kritikal untuk NACA 4412 dan NACA 4418 adalah pada 45° pada kelajuan udara di 20 m/s dan 30 m/s manakala sudut serangan kritikal untuk kedua-dua airfoil berada pada 40 ° pada kelajuan 10 m/s. Kesan ketebalan aerofoil terhadap daya aerodinamik juga dikaji di mana NACA 4418 menjana daya angkat lebih pada sudut serangan terbaik berbanding dengan NACA 4412. Prestasi untuk NACA 4418 adalah lebih baik daripada NACA 4412.

ACKNOWLEDGEMENTS

First and foremost, I would like to give thanks and praises to Almighty God for the blessing and strength that He gave in order for me to fulfill and complete this final year project (FYP).

I would like to express my sincere gratitude to my supervisor, En. Shamsul Bahari Bin Azraai for all of his valuable contribution, guidance, ideas and comments during my journey on finishing this project. Views and opinions from him that allow me to grow and understand more on this project. I also would like to give gratitude to En. Mohd. Hafidzal Bin Mohd. Hanafi and Dr. Md. Isa Bin Ali for their comments and suggestion that help me to improve my project as well as gain more knowledge.

A special thanks to my family members for their love, support and words of encouragement that boost my strength and confidence to complete this project. Besides, I also like say thanks to all my friend that support me throughout this journey that keep me cheerful during tough times. Finally, to everyone who has directly or indirectly contributed to this project, I say thank you as well.

TABLE OF CONTENTS

CHAPTER	TITLE	PAGE
	DECLARATION	
	APPROVAL	
	DEDICATION	
	ABSTRACT	i
	ABSTRAK	ii
	ACKNOWLEDGEMENT	iii
	TABLE OF CONTENTS	iv
	LIST OF FIGURES	vii
	LIST OF TABLES	xi
	LIST OF ABBREVIATIONS	xiii
	LIST OF SYMBOLS	xiv
1	INTRODUCTION	
	1.0 Background of Study	1
	1.1 Problem Statements	4
	1.2 Objective	5
	1.3 Scope of Study	6
	1.4 General Methodology	6

2	LITERATURE REVIEW	
2.0	Introduction	8
2.1	Theory on Aerodynamic Forces and Mathematic Modelling	8
2.1.1	Fluid Flow	8
2.1.2	Lift and Drag Forces	11
2.1.3	Reynolds Number	12
2.2	Applications of Airfoils	12
2.3	Approach in Investigation of Aerodynamic Force on Airfoil	14
2.3.1	Experimental Investigation on Airfoil	14
2.3.2	Numerical Investigation on Airfoil	16
2.3.3	Numerical and Experimental Investigation on Airfoil	16
3	METHODOLOGY	
3.0	Introduction	19
3.1	Modelling Airfoils Geometry in Solidworks 2017	21
3.2	Importing Geometry into DesignModeler	24
3.3	Meshing	24
3.4	Setup for Simulation	26
3.5	Post-Processing	26
4	RESULTS AND DISCUSSION	
4.0	Introduction	28

4.1	Aerodynamic Forces on NACA 4412 and NACA 4418	28
4.1.1	Lift Force on NACA 4412	29
4.1.2	Drag Force on NACA 4412	32
4.1.3	Lift Force on NACA 4418	35
4.1.4	Drag Force on NACA 4418	38
4.2	Comparison Between Results Obtained From S-A Model and Transition SST Model for NACA 4412	41
4.3	Comparison Between Results Obtained From S-A Model and Transition SST Model for NACA 4418	42
4.4	Aerodynamic Forces Comparison Between NACA 4412 and NACA 4418	43
4.5	Visualization of Simulated Airfoils Using Contours	46
4.6	Validation of Data	52
5	CONCLUSION AND RECOMMENDATION	
5.0	Conclusion	55
5.1	Recommendation	56
	REFERANCES	57
	APPENDICES	59

LIST OF FIGURES

FIGURE	TITLE	PAGE
1.1	An airfoil geometry profile. (Source : https://en.wikipedia.org/wiki/Airfoil)	1
1.2	Forces components on an airfoil.	3
1.3	Flow chart of the general methodology	7
2.1	Viscous flow regions and inviscid flow regions on fluid flow over a flat plate. (Cengel & Cimbala, 2009)	9
2.2	Image of laminar, transitional and turbulent flows. (Cengel & Cimbala, 2009)	11
2.3	Lift coefficient versus angle of attack (Ahmad Khairuddin, 2008)	17
2.4	Aerodynamic force obtained by simulation using Transition SST model at 20 m/s by Lim (2009)	18
3.1	Planned flow for CFD simulation.	20
3.2	Coordinate of NACA 4412 airfoil (Left) and NACA 4418 (Right).	22
3.3	3-D Model of NACA 4412 drawn in Solidworks.	23
3.4	3-D Model of NACA 4418 drawn in Solidworks.	23
3.5	Number of nodes, elements and skewness for NACA 4412 at 0°	25
3.6	Meshing done airfoil and the fluid domain	25

3.7	Aerodynamic forces on NACA 4418 at air velocity of 20 m/s and angle of attack of 10° using Transition SST model	27
3.8	Aerodynamic forces on NACA 4412 at air velocity of 30 m/s and angle of attack of 50° using S-A model	27
4.1	Graph of lift force of NACA 4412 using S-A model against different angle of attack at 10 m/s	29
4.2	Graph of lift force of NACA 4412 using SST model against different angle of attack at 10 m/s	29
4.3	Graph of lift force of NACA 4412 against different angle of attack for S-A Model	31
4.4	Graph of lift force of NACA 4412 against different angle of attack for Transition SST Model	32
4.5	Graph of drag force of NACA 4412 using S-A model against different angle of attack at 10 m/s	32
4.6	Graph of drag force of NACA 4412 using Transition SST model against different angle of attack at 10 m/s	33
4.7	Graph of drag force of NACA 4412 against at three different speed and angle of attack for S-A model	34
4.8	Graph of drag force of NACA 4412 against at three different speed and angle of attack for Transition SST model	35
4.9	Graph of lift force of NACA 4418 using S-A model against different angle of attack at 10 m/s	35
4.10	Graph of lift force of NACA 4418 using Transition SST model against different angle of attack at 10 m/s	36
4.11	Graph of lift force of NACA 4418 against different angle of attack for S-A Model	37

4.12	Graph of lift force of NACA 4418 against different angle of attack for Transition SST Model	38
4.13	Graph of drag force of NACA 4418 using S-A model against different angle of attack at 10 m/s	38
4.14	Graph of drag force of NACA 4418 using Transition SST model against different angle of attack at 10 m/s	39
4.15	Graph of drag force of NACA 4418 using S-A model at three different air velocity	40
4.16	Graph of drag force of NACA 4418 using Transition SST model at three different air velocity	40
4.17	Graph of lift force against different angle of attack for S-A and Transition SST Model	41
4.18	Graph of drag force against different angle of attack for S-A and Transition SST Model	42
4.19	Graph of lift force against different angle of attack for S-A and SST Model	42
4.20	Graph of drag force against different angle of attack for S-A and SST Model	43
4.21	Graph of lift force against angle of attack at 30 m/s between NACA 4412 and NACA 4418	44
4.22	Graph of drag force against angle of attack at 30 m/s between NACA 4412 and NACA 4418	45
4.23	Pressure contour at angle of attack, 0°	46
4.24	Velocity contour at angle of attack, 0°	47
4.25	Velocity vector at angle of attack, 0°	47

4.26	Pressure contour at angle of attack, 20°	48
4.27	Velocity contour at angle of attack, 20°	48
4.28	Velocity vector at angle of attack, 20°	49
4.29	Pressure contour at angle of attack, 50°	49
4.30	Velocity contour at angle of attack, 50°	50
4.31	Velocity vector at angle of attack, 50°	51
4.32	Comparison between lift force obtained through simulation with Lim (2009)	52
4.33	Comparison between drag force obtained through simulation with Lim (2009)	53



LIST OF TABLES

TABLE	TITLE	PAGE
3.1	Details of test for the CFD simulations.	19
A.1	Properties of air at 1 atm pressure. (Cengel & Boles, 2015)	59
B.1	US Standard Atmosphere Air Properties – SI Units (Source: https://www.engineeringtoolbox.com/standard-atmosphere-d_604.html)	60
B.2	Table B.2: Linear interpolation.	61
C.1	Gantt chart for PSM I	63
C.2	Gantt chart for PSM II	64
D.1	Results for NACA 4412 at 10 m/s using S-A Model	65
D.2	Results for NACA 4412 at 20 m/s using S-A Model	65
D.3	Results for NACA 4412 at 30 m/s using S-A Model	66
D.4	Results for NACA 4412 at 10 m/s using SST Model	66
D.5	Results for NACA 4412 at 20 m/s using SST Model	67
D.6	Results for NACA 4412 at 30 m/s using SST Model	67
E.1	Results for NACA 4418 at 10 m/s using S-A Model	68
E.2	Results for NACA 4418 at 20 m/s using S-A Model	68
E.3	Results for NACA 4418 at 30 m/s using S-A Model	69

E.4	Results for NACA 4418 at 10 m/s using SST Model	69
E.5	Results for NACA 4418 at 20 m/s using SST Model	70
E.6	Results for NACA 4418 at 30 m/s using SST Model	70



LIST OF ABBREVIATIONS

NACA	=	National Advisory Committee for Aeronautics
CFD	=	Computational Fluid Dynamic
3-D	=	3-Dimensional
S-A	=	Spalart-Allmaras
SST	=	Shear Stress Transport
FKM	=	Fakulti Kejuruteraan Mekanikal @ Faculty of Mechanical Engineering
UTeM	=	Universiti Teknikal Malaysia Melaka



LIST OF SYMBOLS

α	=	Angle of attack
x_0, y_0, z_0	=	Fixed point in the fluid field
V	=	Upstream velocity (m/s)
P	=	Pressure (Pa)
t	=	Time (s)
Ma	=	Mach Number
F_D	=	Drag force (N)
F_L	=	Lift force (N)
ρ	=	Density (kg/m ³)
C_D	=	Coefficient of drag
C_L	=	Coefficient of lift
Re	=	Reynolds Number
L_c	=	Chord length of airfoil (m)
μ	=	Dynamic viscosity of fluid (kg/m.s)
ν	=	Kinematic viscosity of fluid (m ² /s)
H	=	Altitude (m)
T	=	Temperature (°C)

CHAPTER 1

INTRODUCTION

1.0 Background of Study

An airfoil is defined as the cross section of a body that is placed in an airstream to produce a useful aerodynamic force in the most efficient manner possible. (E. Abrahams & D. Cladwell, 2005) The airfoil profile geometry is shown in Figure 1.1. The important aspects of the airfoil geometry are the maximum camber, chord and the maximum thickness where it is used for classification of an airfoil. The length of the chord line that connecting the leading and trailing edges is called chord. Leading edge is the point at front of the airfoil that has maximum curvature whereas the trailing edge is the point has maximum curvature as well but at the rear area of the airfoil. The maximum camber line is the distance between the mean camber line and the chord. The thickest part of the airfoil is the maximum thickness.

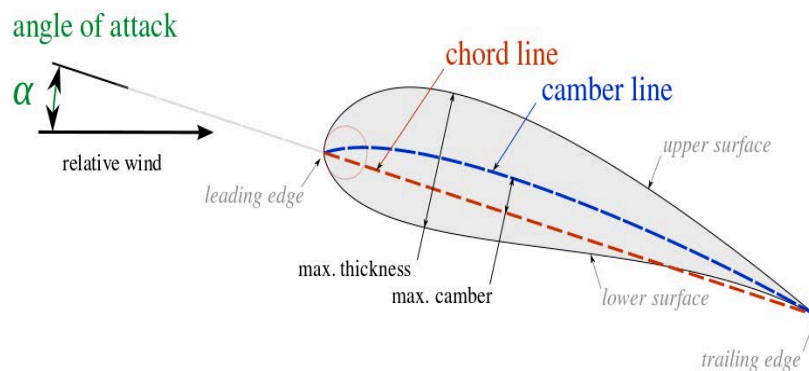


Figure 1.1: An airfoil geometry profile. (Source: <https://en.wikipedia.org/wiki/Airfoil>)

One of the common and known airfoils throughout the world of aviation is NACA airfoil. NACA airfoils are series of airfoils developed by the National Advisory Committee for Aeronautics (NACA); hence, the name given to the airfoils. NACA has standardized the group of airfoils into 4-digit, 5-digit and 6-digit series and the meaning of this nomenclature are best explained by examples.

NACA 2412

2 → The mean line has a camber of 0.02 chord; mean line has 4 % camber

4 → The maximum camber located at 0.4 chord

12 → The maximum thickness is 0.12 chord, airfoil has 12% thickness

NACA 23012

2 → The mean chamber line has a camber of 0.02 chord approximately

30 → The maximum camber is located at $0.3/2 = 0.15$ chord

12 → The maximum thickness is 0.12 chord.

NACA 65₃ - 418

6 → Series designation

5 → The minimum pressure point is at 0.5 chord

3 → The minimum drag coefficient occurs at an angle of attack that corresponds to the design lift coefficient and the bucket-like shape of drag curve (drag bucket) stretches from design lift coefficient of -0.3 to +0.3

3 → design lift coefficient is 0.4

18 → The maximum thickness is 0.18 chord

These are the primary airfoils' series that introduced by the NACA but this does not include the modified series and the airfoils used for supersonic flight. All airfoils have their own unique flight characteristics so the factor of choosing an airfoil usually depends on the requirement for the experiment or manufacturers of the aircraft wings and turbines. Yeminici O. (2014) chose NACA 0012 for his study because of the symmetrical shape of NACA 0012. Kamas T. (2009) chooses the symmetrical NACA 0012 and the cambered NACA 2414 in his study the aerodynamic forces effect on those airfoils.

Aerodynamic forces are forces exerted on a body by the air where the body is immersed in air and it is due to the flow between the body and the gas. When airflow through an airfoil, aerodynamic forces are created caused by normal force and shear force. The normal force is due to the pressure surrounding the airfoil and the skin friction due to the viscosity of the air. The aerodynamic forces in an airfoil can be resolved into three different components with the addition of weight as shown in Figure 1.2. Weight is not considered as an aerodynamic force but a body force since it is caused by gravity and not exerted on the body by air. The lift force is the component of the force that is perpendicular to the flow direction of air while drag force is parallel to the direction of the air flow. Drag is the force that resists the motion of an aircraft during flight. Thrust is the forward force created by the jet engines or propellers to overcome the drag force and thus it acts in the opposite direction of drag force.

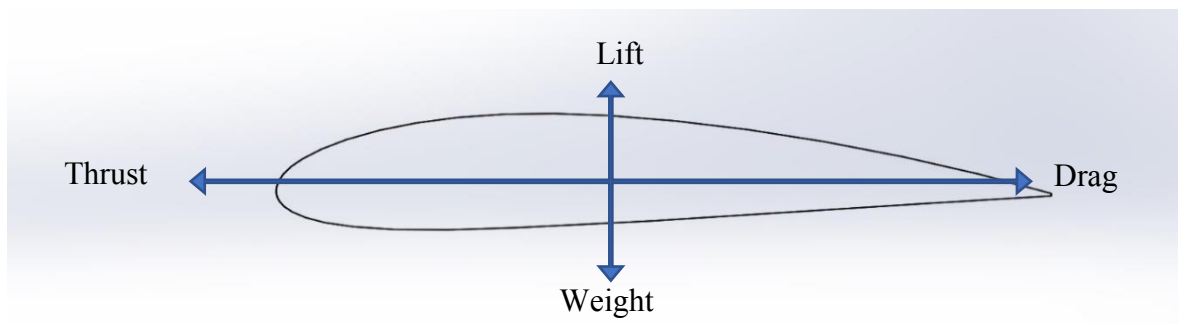
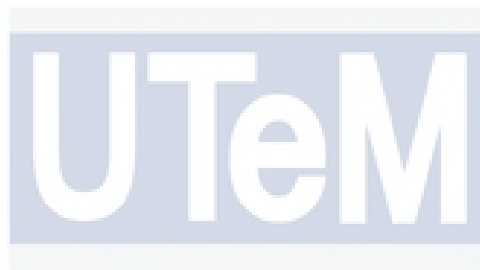


Figure 1.2: Forces components on an airfoil.

An airfoil is designed in a way that the shape takes advantage of the air to react to certain laws of physics. A positive pressure lifting action occurs at the lower surface of the airfoil and a negative pressure lifting action from lowered pressure on the top surface occurs as the air strikes the airfoil. In an aircraft flight or in a wind tunnel, an airfoil is a streamlined object that is placed into an airstream movement. For the airfoil to lift, the air moving over the upper surface must move faster than the air moving along the lower surface. This is done by inclining the airfoil to a certain angle so that the airflow becomes faster at the upper surface. The increase in speed on the upper surface of the airfoil produces a drop in pressure according to Bernoulli's principle. This will cause differences in pressure on upper and lower surface. The higher pressure on the lower surface will push the airfoil upward and thus creating lift force.



1.1 Problem Statement

Fuel consumption in an airplane is the major problem for the airline companies and aircraft manufacturers. Koppula, R (2018) stated that it has been estimated that fuel demands from aviation will increase by between 1.9% and 2.6% each year until 2025. This means that more money will be spent on the fuel for the aircraft to operate. Most airline companies and aircraft manufacturer want to reduce the amount of money spend on fuel consumption of aircraft. Fuel consumption can be related to the drag produced by the aircraft during flight. If the drag produced by the aircraft high, the fuel consumption also increases.

This is because of the thrust needed to overcome the drag is produced by the engines of the aircraft. The engines used fuel to power up thus the drag indirectly increased the fuel consumption. Payloads of the aircraft also play an important role in fuel consumption but in this study, the concern is more toward reducing the drag to increase the efficiency of fuel

consumption. Reducing drag means that study on airfoils essential for correct selection of airfoils needed to design the wing, winglet and the tail plane.

Haque M. N., et al. (2015) stated that the efficiency, as well as the performance of an aircraft mostly depend on the aerodynamic characteristics e.g. lift, drag, lift to drag ratio, etc. of wings. Therefore, improving the aerodynamic characteristics are desired by the aircraft manufacturers and racing cars company. Airfoils geometry such as the maximum thickness and maximum camber can play an important role in order to improve the aerodynamic forces. The different in geometry might able to generate significant lift or reducing drag that can improve the aerodynamic performance of the airfoils before selecting it for use of aircraft or the geometry able to help to increase the down force for racing car to increase it speed.

An aerodynamic stall also a concern when flying an airplane. An aerodynamic stall is a condition when the airfoil exceeds its critical angle of attack and cannot produce the desired lift force for the flight. An aerodynamic stall can cause a sudden change in the airplane level where it feels like the airplane is falling. Besides, it also can cause the airplane to roll or turn to one side of the airplane. It a dangerous condition since aircraft may enter a spin and the pilot lose control of the airplane. Therefore, knowing the critical angle of an airfoil is important when designing the aircraft's wings, horizontal and vertical stabilizers.

1.2 Objectives

- i. Comparing the aerodynamic forces between two different NACA airfoil on Computational Fluid Dynamic (CFD) simulation with different turbulent models.
- ii. Analyze the best angle of attack on the airfoils at different velocities

- iii. Study the effect of the maximum thickness of the geometry of airfoils toward the aerodynamic forces

1.3 Scope of Study

This study covers the Computational Fluid Dynamic (CFD) simulation to investigate the aerodynamic forces on two different NACA airfoils. ANSYS Fluent 16 software was used to simulate the CFD simulation with two different turbulence model which are Spalart-Almaras (S-A) turbulence model and Transition Shear Stress Transport (SST) model. The simulation done in three different air velocity of 10 m/s, 20 m/s and 30 m/s at varying angle of attack ranging from 0° to 50° with increment of 5° . The airfoils are drawn using Computer Aided Design (CAD) software with chord length of 10 cm. The aerodynamic forces from the results obtained in both simulation of airfoils will be analyzed and compared.

1.4 General Methodology

The steps and details that are needed to be done to achieve the objectives of the study are discussed in this section. The steps are shown below:

1. Literature review

Reviewing journals, articles, books and any other materials that are related to the study to collect data.

2. CAD drawing on the chosen NACA airfoils

Draw the NACA airfoil according to the specification on the NACA tool website. The drawing then will be tested for CFD simulation and it will be fabricated by a 3-D printer for the experiment.

3. CFD simulation

Simulation using different turbulence models on ANSYS Fluent on the NACA airfoil and get the results in term of lift coefficients, drag coefficient and lift to drag ratio at a certain angle of attack.

4. Analysis

All the results are tabulated in the graph. Comparison and analysis of the results are will be done.

5. Report writing

Report on the study will be written at end of the study to show the progress of the study and the end results of the investigation.

The methodology can be summarized in a flow chart shown in Figure 1.3.

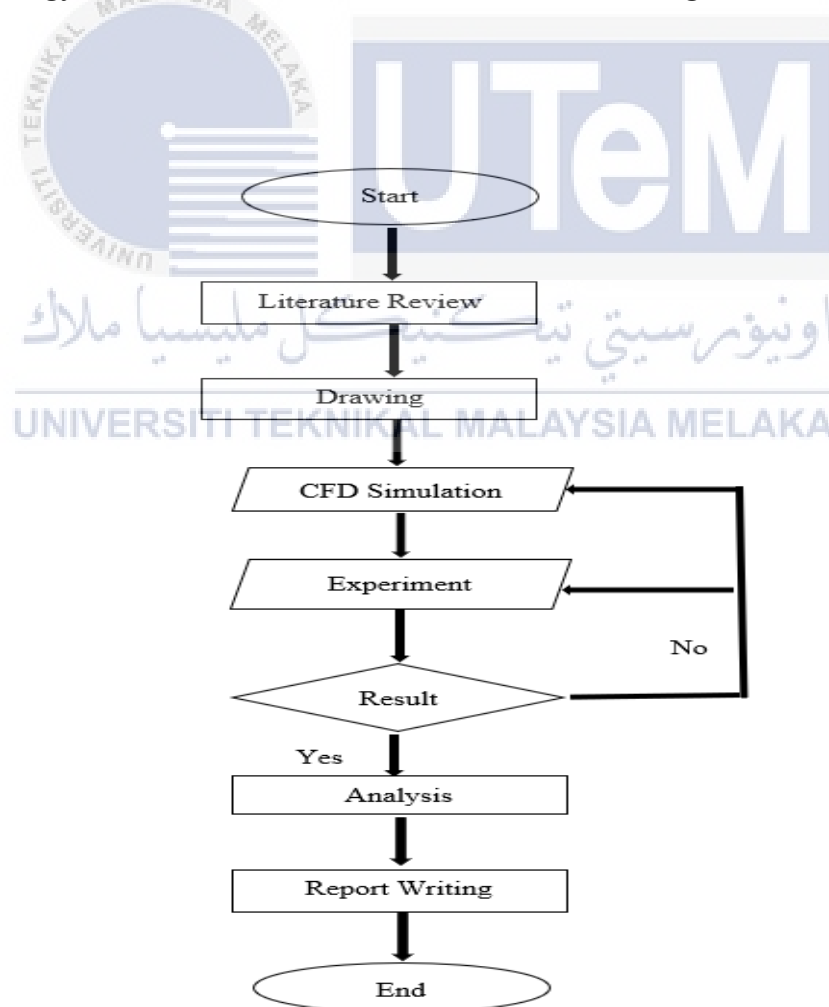


Figure 1.3: Flow chart of the general methodology

CHAPTER 2

LITERATURE REVIEW

2.0 Introduction

This chapter discussed the previous research and sources related to the investigation of aerodynamic forces on the airfoils. The sources include journals, articles, report, book, and websites. The sources are used as a guideline to complete this study by using the related information, ideas and knowledge obtained from it. In this study, theories and mathematical modeling related to the investigation of the aerodynamic forces on airfoils is discussed. Besides, the history of airfoil early development and the applications of airfoils are also discussed. The type of investigation approach also discussed in this chapter.

2.1 Theory on Aerodynamic and Mathematic Modeling

2.1.1 Fluid Flow

Fluid is a substance in the phase of liquid or gas. The flow of a fluid can be categorized through some common characteristics so that it will be easier to identify the type of fluid flow. Fluid flow can be either steady or unsteady flow. According to R.K. Bansal, steady flow is described as the kind of flow where the fluid features like velocity, pressure, density, and many more at a point do change with time. This can be described mathematically, where

$$\left(\frac{\partial v}{\partial t}\right)_{x_0, y_0, z_0} = \left(\frac{\partial p}{\partial t}\right)_{x_0, y_0, z_0} = \left(\frac{\partial \rho}{\partial t}\right)_{x_0, y_0, z_0} = 0 \quad (2.1)$$

Where x_0, y_0, z_0 is a fixed point in the fluid field.

He also states that unsteady flow is that type of flow, in which the speed, pressure, density at a point changes with respect to time. Mathematically, unsteady flow can be described as

$$\left(\frac{\partial v}{\partial t}\right)_{x_0, y_0, z_0} \neq 0, \quad \left(\frac{\partial p}{\partial t}\right)_{x_0, y_0, z_0} \neq 0 \quad (2.2)$$

Fluid flow can be categorized as inviscid and viscous flow. Viscosity is a fluid property that representing the internal resistance of fluid where it is due to the frictional force that appears between different layers of fluids as they forced to move relative to each other. Cengel, Y. A. and Cimbala, J. M. (2009) stated that flow in which the frictional effects is significant are called viscous flows. Inviscid flow is where the frictional effects less significant in the fluid flow. Both of this flow can be represented by regions when fluid flow over a flat plate and viscous regions located near to the body on both sides while the inviscid flow regions are away from the flat plate on both sides. This is shown in Figure 2.1.



Figure 2.1: Viscous flow regions and inviscid flow regions on fluid flow over a flat plate.

(Cengel & Cimbala, 2009)

Fluid flow also can be categorized depending on whether the flow is confined in a channel or it is flowing over a surface of a body. The flow over a body's surface is called external flow while the flow is called internal flow when it flows inside a channel. The

example of internal fluid flow is the flow of water inside a pipe. As for external flow, the wind flow over wind turbines.

Moreover, fluid also can be categorized as compressible and incompressible depend on the density of the fluid during the flow. A flow is categorized as incompressible if the density of the fluid remains nearly constant whereas the flow is compressible if the density opposite of the incompressible flow. Flow involving liquid flows are usually incompressible while the gas flows often compressible typically in high speeds. According to Cengel, Y. A. and Cimbala, J. M. (2009), the flow speed is often expressed in terms of dimensionless Mach number when analyzing systems that involved a high-speed gas flow. Mach Number defined as $Ma = V/c$ where V is the flow's speed while c is the speed of sound which the value is 346 m/s in the air at room temperature at sea level. Mach number also acts as an indicator of whether the compressibility effects are important. The value of Mach number indicates,

$Ma < 0.3$: Incompressible

$Ma < 1$: Subsonic

$Ma = 1$: Sonic

$Ma > 1$: Supersonic

$Ma \gg 1$: Hypersonic

Fluid flows also can be characterized by the fluid motion which is laminar, transitional and turbulent flow. Laminar flows are smooth and orderly fluid motion while turbulent flows are described as chaotic or disorder fluid motion. Laminar flows usually occur in low velocities while turbulent flows occur in high velocities. Transitional flows are the flows between laminar and turbulent. The flows can be seen in Figure 2.2 so that it is easier to be described.

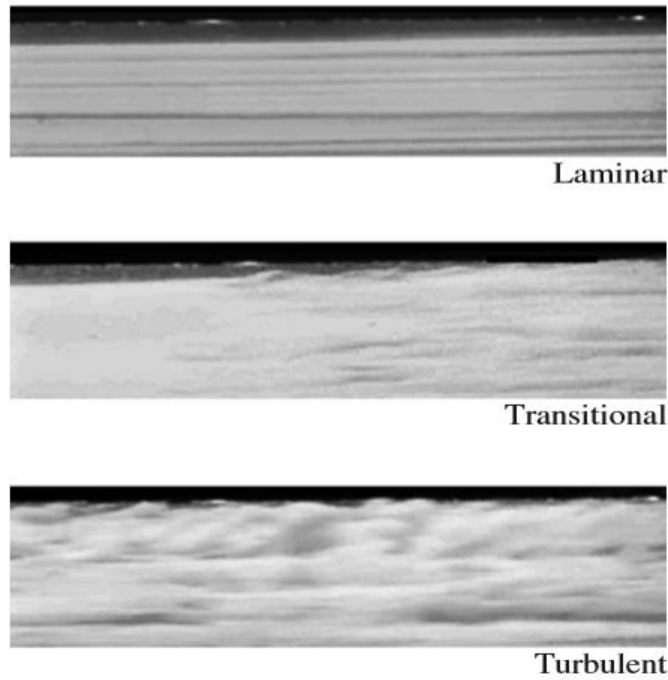


Figure 2.2: Image of laminar, transitional and turbulent flows. (Cengel & Cimbala, 2009)

2.1.2 Lift and Drag Forces

Drag is the resultant force in the direction of upstream velocity, and it is due both skin frictions drag, D_f or pressure drag, D_p . Skin friction drag is due to wall shear stress occurring in a fluid when it flows over a body while pressure drag is due to differences in pressure on the front and rear of a body. According to Cengel, Y. A. and Cimbala, J. M. (2009), the components of the pressure and wall shear forces in normal direction is lift. The formula for lift force and drag are listed in equation below:

$$F_D = \frac{1}{2} \rho L_C V^2 C_D \quad (2.3)$$

$$\text{Thus, } C_D = F_D / \frac{1}{2} \rho L_C V^2 \quad (2.4)$$

$$F_L = \frac{1}{2} \rho L_C V^2 C_L \quad (2.5)$$

$$\text{Thus, } C_L = F_L / \frac{1}{2} \rho L_C V^2 \quad (2.6)$$

2.1.3 Reynolds Number

Reynolds number, Re is a dimensionless quantity and it is the ratio of inertial forces to viscous forces inside a fluid. It is used to estimate the flow patterns in different fluid flow.

$$Re = \frac{\rho V L c}{\mu} = \frac{V L c}{\nu} \quad (2.12)$$

2.2 Applications of Airfoils

The interest of this study is to investigate the NACA airfoil mainly for the application in aircraft. This interest is important to help the improvement of the design of aircraft since the production of aircraft fleet has been increased throughout the years. The global fleet is expected to grow by 20,930 aircraft to reach about 40,000 in total 2032. (Koppula, R., 2018) Increase in production means fuel consumption would be a major problem in aviation business because fuel is quite expensive and carbon dioxide emission from the burning of the fuel contributes to global warming.

The design of airfoil helps in enhancing the aerodynamic performance which help in flight efficiency. The flight efficiency helps to reduce thrust needed to overcome the drag produced by aircraft. Thrust is produced by burning of fuel in the engine, therefore, reduction of thrust needed mean that less fuel consumption needed. This is because improvement can help in increasing the fuel efficiency used by aircraft. Fuel cost is a problem since most aircraft need a huge gallon of fuel per trips. Fuel consumption can also lead to increase in carbon dioxide emission to the surroundings.

Al-Kayiem, H. H., & Kartigesh, A. K. (2011) studied the aerodynamic characteristic of an airfoil in a ground collision because of problem due to the wing-ground collision. The

study involved experimental and numerical investigation of NACA 4412 airfoil. The NACA 4412 model with 105 mm chord length was tested in low-speed subsonic wind tunnel with test section of 300mm x 300mm. The numerical analysis was done with CFD based on the discretization of the domain and the governing equations of the flow field. RNG k-epsilon turbulent model was used to generate the turbulent flow in the study.

Airfoils also commonly used in the designing blade of a wind turbine. It a crucial part in order to generate electricity through wind power. The wind turbine airfoils use the concept as the airfoils used in aircraft. Fatehi, M., et al. (2019) investigate the use of cavity shape optimization to enhance the aerodynamic performance of a Riso_B1_18 airfoil which used for a wind turbine blade. The study compares the Riso airfoil with and without the optimized cavity through experimental and numerical investigation.

Wang, Y., et al. (2018) also studied on the aerodynamic performance of vertical axis wind turbine with different series of airfoil shapes. The airfoils can be categories by 1. Symmetrical airfoils with the same maximum thickness positions, but different maximum thickness; 2. symmetrical airfoils with same thickness, but different maximum thickness positions; 3. non-symmetrical airfoils with same maximum thickness, same maximum thickness position, same maximum camber position, but different maximum cambers; 4. Non-symmetrical airfoils with same maximum thickness, same maximum thickness position, same maximum camber, but different maximum camber positions. This study uses the numerical investigation approach to obtain the aerodynamic performance of the wind turbine.

The application of airfoils in the automobile industry is important since the airfoil help to give downforce to the car. An automotive airfoil is shaped like an upside-down airplane wing; it deflects airflow upward to generate down-force on the rear of the vehicle.

(Q, 2016) More downforce means that the car became more stable when it is accelerating. Airfoils mostly used in racing car wings especially the Formula 1 car's front and rear wing. Durrer S. (2016) study the behavior of a race car wing that operating in a wake. Operating in wake referring to when the race car following another car. The airfoil model used in this study was Selig's S1223 airfoil which has high lift profile. A CFD study on the airfoil was done and he found that different parameters such as velocity, ground clearance, the angle of attack and distance between a car and a wing influence the aerodynamic forces.

2.3 Approach in Investigation of Aerodynamic Force on Airfoil

In investigating the aerodynamic forces on NACA airfoils, there are two types of investigation that usually done by researchers across the world. The investigations are the experimental and numerical investigation. Some researchers use the numerical investigation or experimental investigation only, but some also chosen to do both investigations. In this study, both types of investigation are used to study the mechanism used for the investigations and make a comparison between the two type of investigation approach.

2.3.1 Experimental Investigation on Airfoil

An experimental investigation is a traditional technique in investigating the fluid flow around the airfoils. It has better accuracy compared to the numerical investigation because it happened in actual conditions, and the data obtained are not guessed or predicted. An experimental investigation would take a longer time to be done and higher cost to buy the equipment needed. This is because the experiment usually was done in a wind tunnel and model needed to perform the experiment, so money is needed in order to perform it. In order to obtained accurate data, the time needed to try and error on the experiment. Experiment in

wind tunnel reverses the process that occurs in a real application, where the aircraft move against the air. In the wind tunnel, the model is placed on a stand while the air moves at certain speed past the model.

Haque, M. N., et al. (2015) used the experimental investigation to explore better aerodynamic performance by incorporating curvature to the leading edge of an aircraft wing. They investigate aerodynamic performance of NACA 4412 by comparing two models of rectangular planform NACA 4412 and a curved leading edge with straight trailing edge NACA 4412. Both models are equal in length and surface area and tested in a closed-circuit wind tunnel with Re of 1.82×10^5 , static pressure at a different angle of attack of -4° , 0° , 4° , 8° , 12° , 16° , 20° , and 24° . They found that the lift coefficient of the curved leading edge planform increases and the drag coefficient decreases at angles of attack below 12° compared to the rectangular planform but after the critical angle of attack, the values do not vary significantly. So, the aerodynamic performance of curved leading edge planform of NACA 4412 is better than the rectangular planform below the critical angle of attack.

D'souza, A. G., et al (2015) also used experimental investigation in low-speed wind tunnel for their study. Low-speed wind tunnel or subsonic wind tunnel was used to study the NACA 4412 design parameters which can affect the lift and drag coefficients. The model has 20 cm chord length and 5 inches thick. The model was tested at a wind speed of 35 m/s and angle of attack of 0° . The study tests the stability of the wind tunnel by testing the stability of the hydrodynamic boundary layer throughout the test section. Flow visualization was conducted where the flow remained unseparated throughout the test section at 70 % of the characteristic dimension of the section during the testing with the airfoil. Smooth visible flow separation was observed when the airfoil was removed.

2.3.2 Numerical Investigation on Airfoil

Numerical investigation approaches used CFD to solve the algebraic equation for the fluid flow around the airfoil. The advantages of this approach would be the cheaper in cost and faster time taken to obtain the flow around the airfoil. It also can be used for all desired quantities with high-resolution prediction of a virtual problem with the realistic operating condition. The main concern for this approach is the validation and reliability of the results obtained. This is because input data may involve imprecision and estimation and the computer specification also may affecting the accuracy of the results obtained.

Kevadiya, M. & Vaidya, H. (2013) also studied on NACA 4412 by doing CFD analysis on the airfoil. The airfoil is modeled in GAMBIT 2.4.6 software with a chord length of 0.1m. The CFD analysis was done using FLUENT 6.3.26 at angles of attack varied from 0° to 12° and Reynolds number of 1×10^5 . The solver was pressure based steady state with the viscous model using the Spalart-Allmaras model used. The inlet velocity is set at 18m/s and the viscosity set at 1.7894. They found that the stall angle is at 8° since the lift to drag ratio decreased after that.



2.3.3 Numerical and Experimental Investigation on Airfoil

The numerical and experimental approach may be expensive and time-consuming, but the data obtained will be more accurate and the results from both approaches can be compared and validated. Through doing both investigations, researchers can see the differences in the approach and make a comparison that can be useful for future researcher's references.

Ahmad Khairuddin (2008) studied on NACA 4412 by doing CFD simulation and experiment at air speed of 46 m/s and different angle of attack. The angle of attack ranging from -4° to 22.5° . The CFD simulations were done in two type of software which are ANSYS

FLUENT and GAMBIT while the experiment was done in wind tunnel with test section of 300mm x 300 mm x 1500mm. The chord length for the airfoil used was 105 mm. From the ANSYS FLUENT analysis and the experiment, the stall angle at angle of the airfoil obtained is at 22.5°. Figure 2.3 show the result obtain through the simulation on ANSYS fluent.

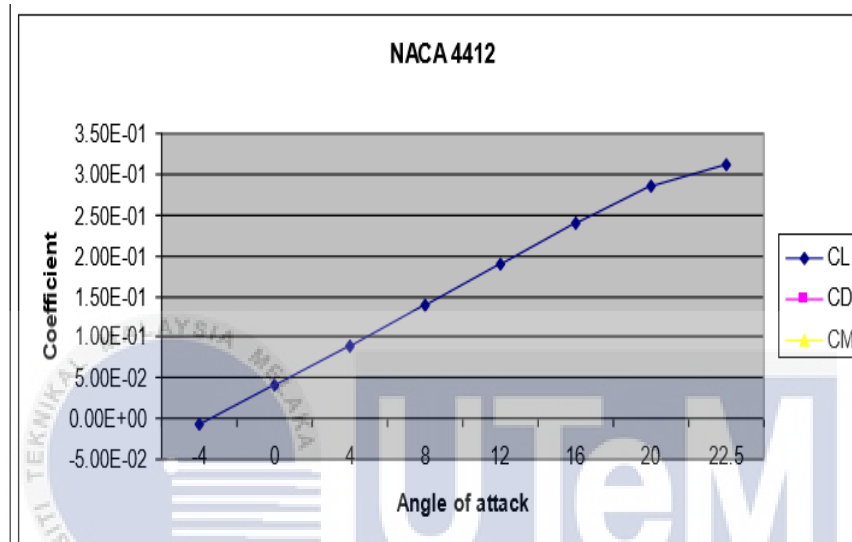


Figure 2.3: Lift coefficient versus angle of attack (Ahmad Khairuddin, 2008)

Lim F. K. (2009) studied about the air flow for NACA 2412 and NACA 4412 through simulation using ANSYS CFX and experiment in wind tunnel. The aim for his study is to find drag force acting on the airfoil and determine which airfoil has better performance. Both airfoils have chord length of 100 mm and the airfoils are tested in three different air speed of 10 m/s, 20 m/s and 30 m/s. The angle of attack for the airfoil are increase by 5° in each for each of the velocity tested which range from 0° to 50°. For CFD simulations, Transition SST model were used as the turbulence model. The lift and drag force obtained is shown in Figure 2.4.

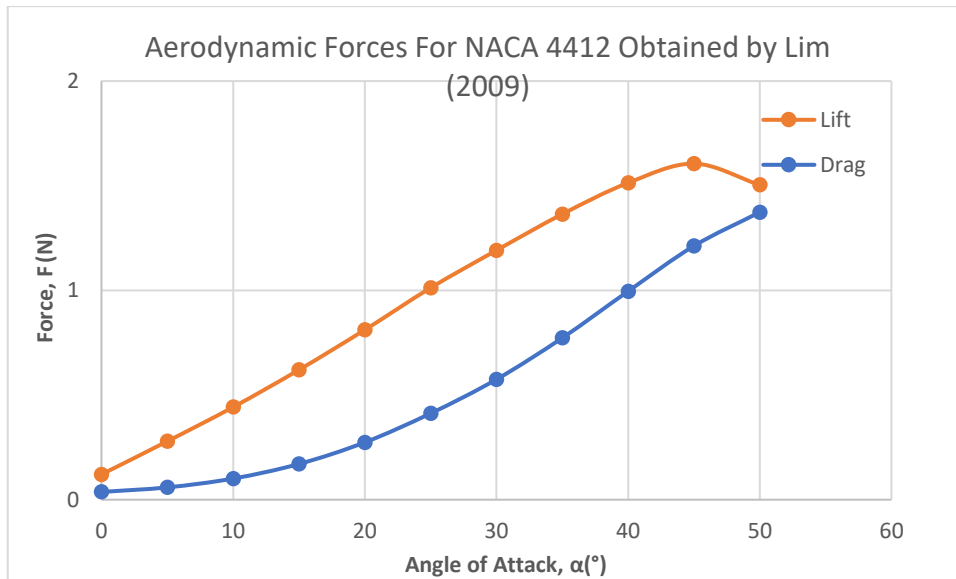
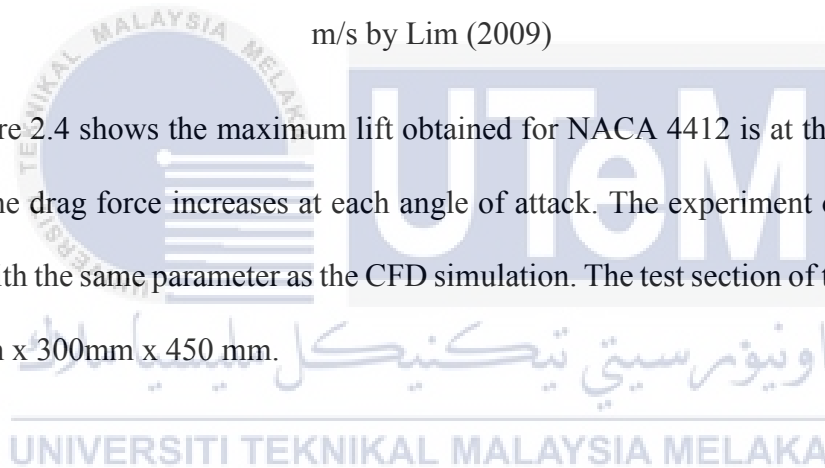


Figure 2.4: Aerodynamic force obtained by simulation using Transition SST model at 20 m/s by Lim (2009)

Figure 2.4 shows the maximum lift obtained for NACA 4412 is at the stall angle of 45° while the drag force increases at each angle of attack. The experiment on wind tunnel was done with the same parameter as the CFD simulation. The test section of the wind tunnel is at 300mm x 300mm x 450 mm.



CHAPTER 3

METHODOLOGY

3.0 Introduction

This chapter describe the methodology used in this study to obtain the desired results. NACA 4412 and NACA 4418 are chosen to be tested in this study. CFD simulation using ANSYS FLUENT software is used to virtually test the airfoils. The tests are done to determine the stall angle at different velocities for both airfoils and it is done to compare which airfoil is better in term of aerodynamic forces around an airfoil. The chosen airfoils for this study are NACA 4412 and NACA 4418 from the NACA 4-digit series. Both are chosen because both have unsymmetrical shape, same mean camber line and maximum camber but both have different maximum thickness. NACA 4412 has a maximum thickness of 12% at 30% chord while NACA 4418 has a maximum thickness of 18% at 30% of chord.

Table 3.1: Details of test for the CFD simulations.

Test Number	Turbulent Model	Air Velocity, (m/s)	Reynolds Number Based on Chord Length	Angle of Attacks (°)
Test 1	Spalart-Allmaras (SA) Model	10	64020	0°, 5°, 10°, 15°, 20°, 25°, 30°, 35°, 40°, 45° and 50°
		20	128041	
		30	192061	
Test 2	Shear Stress Transport (SST) Model	10	64020	0°, 5°, 10°, 15°, 20°, 25°, 30°, 35°, 40°, 45° and 50°
		20	128041	
		30	192061	

The simulations were done in three different velocity that range from 10 m/s to 30 m/s. The angle of attacks of the airfoils in each different velocity are varied from 0° to 50°. The simulations were done in three different turbulent model which are Spalart-Allmaras (S-A) and shear stress transport (SST) model. The details in shown in Table 3.1. The air is assumed to be at 25°C and the properties taken from property tables and charts shown in Appendix A. The properties table is taken from Thermodynamics: An Engineering Approach book by Cengel. Y. A. and Boles, M. A. (2015).

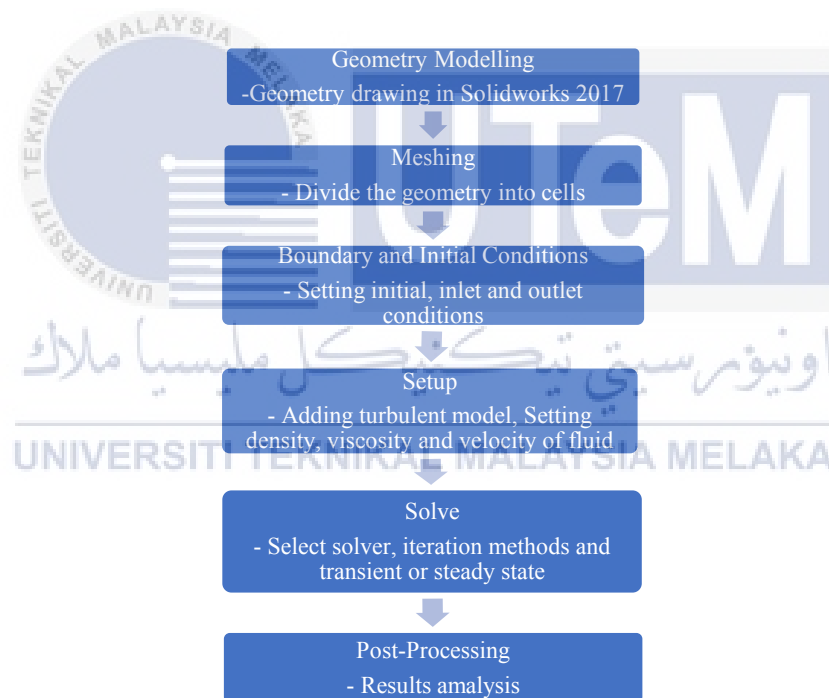


Figure 3.1: Planned flow for CFD simulation.

The simulations for CFD are plan according to the flow chart as shown in Figure 3.1 so that the simulation work smoothly without any problems. The geometry for both airfoils is drawn in Solidworks 2017 while the CFD simulation are done in ANSYS FLUENT 16.

3.1 Modelling Airfoils Geometry in Solidworks 2017

The similarity for the model is done and compare to wing of Jabiru J250 LSA. The similarity deems to be incomplete similarity due to length of model propose on the similarity is large. It is unable to be 3D printed in FKM's Prototype Lab and test in FKM's wind tunnel in the Turbo Machinery Lab. The size become the constraint for the propose model. Initially, experiment on wind tunnel was proposed for this project but it was cancelled due to lift measurement device for the wind tunnel broken and unable to be used. Thus, the model with dimension of 100 mm chord length and 100 mm width chosen to be tested for the simulation as it was initially proposed for the experiment on the wind tunnel. The calculation for the similarity between model and prototype is shown in Appendix B.

The data and coordinate of these airfoils can be obtained from airfoil tools website (<http://airfoiltools.com>). The Selig format dat. file was copied from the website and place in excel and to break the coordinate in columns of X, Y, and Z. Then multiple the coordinates with 100 in order to make the chord length equal to 100 mm. The reason for this is because it will be easier to draw the airfoil with the correct coordinate without the need to change the chord length in Solidworks Premium 2017 Edition. Changing it in Solidworks also might slightly alter the angle of attack and the coordinate of the airfoils.

x	Y	Z	x	Y	Z
100	0.13	0	100	0.19	0
95	1.47	0	95	1.89	0
90	2.71	0	90	3.46	0
80	4.89	0	80	6.22	0
70	6.69	0	70	8.55	0
60	8.14	0	60	10.44	0
50	9.19	0	50	11.85	0
40	9.8	0	40	12.7	0
30	9.76	0	30	12.76	0
25	9.41	0	25	12.4	0
20	8.8	0	20	11.72	0
15	7.89	0	15	10.66	0
10	6.59	0	10	9.11	0
7.5	5.76	0	7.5	8.06	0
5	4.73	0	5	6.75	0
2.5	3.39	0	2.5	5	0
1.25	2.44	0	1.25	3.76	0
0	0	0	0	0	0
1.25	-1.43	0	1.25	-2.11	0
2.5	-1.95	0	2.5	-2.99	0
5	-2.49	0	5	-4.06	0
7.5	-2.74	0	7.5	-4.67	0
10	-2.86	0	10	-5.06	0
15	-2.88	0	15	-5.49	0
20	-2.74	0	20	-5.56	0
25	-2.5	0	25	-5.49	0
30	-2.26	0	30	-5.26	0
40	-1.8	0	40	-4.7	0
50	-1.4	0	50	-4.02	0
60	-1	0	60	-3.24	0
70	-0.65	0	70	-2.45	0
80	-0.39	0	80	-1.67	0
90	-0.22	0	90	-0.93	0
95	-0.16	0	95	-0.55	0
100	-0.13	0	100	-0.19	0

Figure 3.2: Coordinate of NACA 4412 airfoil (Left) and NACA 4418 (Right).

The final coordinate is shown in Figure 3.2. The excel then save as text (tab delimited) format because Solidworks able to read the data save in that format. The text file is inserted to Solidworks via curve through XYZ points and airfoil can be constructed from the coordinate on the text file. When the airfoil already constructed, check the trailing edge to make sure it connected. For both NACA 4412 NACA 4418 airfoils, the trailing edge is not connected. The trailing edge must be connected by drawing a line connecting the trailing edge.

The chord length of both airfoils is defined as 10 cm and the 2-D geometry then will be extruded in order to make it 3-D with width of 10 cm. The sketched airfoil will be used in the ANSYS software for simulation and must be save in IGES file (*.IGS). The 3-D

drawing for NACA 4412 airfoil shown in Figure 3.3 and drawing for NACA 4418 is shown in Figure 3.4.

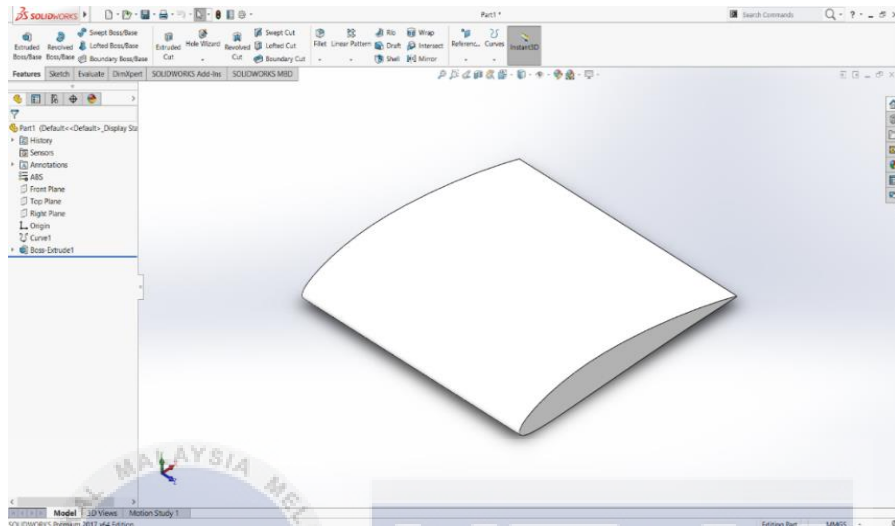


Figure 3.3: 3-D Model of NACA 4412 drawn in Solidworks.

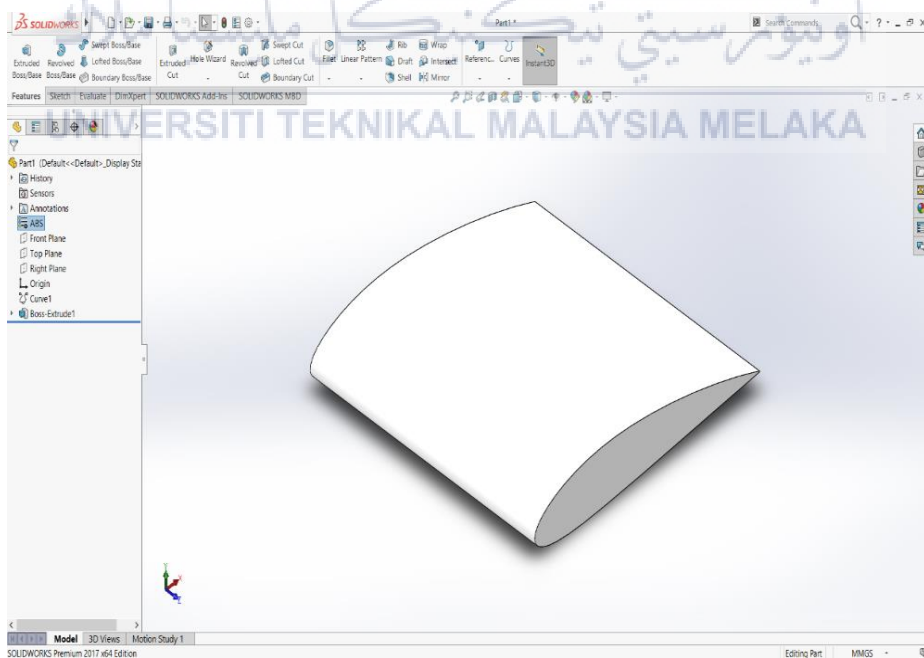


Figure 3.4: 3-D Model of NACA 4418 drawn in Solidworks

3.2 Importing Geometry into DesignModeler

The IGES file of airfoils from Solidworks 2017 can be upload into ANSYS FIUENT workbench by pressing right click on the Geometry and select Import Geometry to browse for IGES file containing the drawing of the airfoils. After choosing the file needed, right click on the Geometry feature and select Edit Geometry in DesignModeler to generate the airfoil geometry in the DesignModeler. The airfoil can be rotated by using Create function inside the DesignModeler and choose body transformation where there is a rotate function. The angle is rotated in local z-axis of the airfoil.

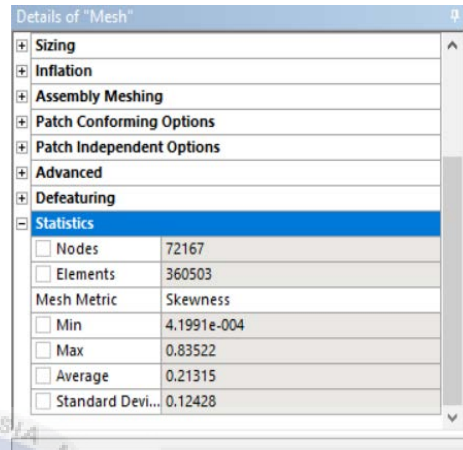
The domain of the airfoil can be created by creating a box with dimension of 300 mm width, 300 mm height and 450 mm long. The box domain was defined as fluid where the the airfoil will be immersed inside the domain to see the fluid flow inside. The dimension of box enclosure is like the test section of FKM's wind tunnel since the test section will enclose the airfoil during the testing.

3.3 Meshing

Meshing were done differently on the airfoils and the domain. This is because the critical part to be mesh would be the airfoil. Body sizing were done on the airfoil with the element size of 2 mm so that there are a lots number of cells at that area for better simulation. The behavior for the body sizing is choose to hard so that the surrounding cells follow the size defined and not changing it.

The general mesh was done on the domain where the relevance center is medium and the size of cells are set as default. Figure 3.6 shows the skewness, number of nodes and elements of NACA 4412 at 0°. The skewness for the meshing ranging from 0.80966 to 0.83522 for both airfoils. The number of nodes is ranging from 72167 to 79076 while the

number of elements is ranging from 360503 to 371264 for both airfoils. The number of nodes and elements are different in each mesh because in each process, the computer generate it differently even if it has the same geometry. This make each simulation unique and different.



The screenshot shows the 'Details of "Mesh"' window in ANSYS. The 'Statistics' section is expanded, displaying the following data:

Property	Value
Nodes	72167
Elements	360503
Mesh Metric	Skewness
Min	4.1991e-004
Max	0.83522
Average	0.21315
Standard Devi...	0.12428

Figure 3.5: Number of nodes, elements and skewness for NACA 4412 at 0°

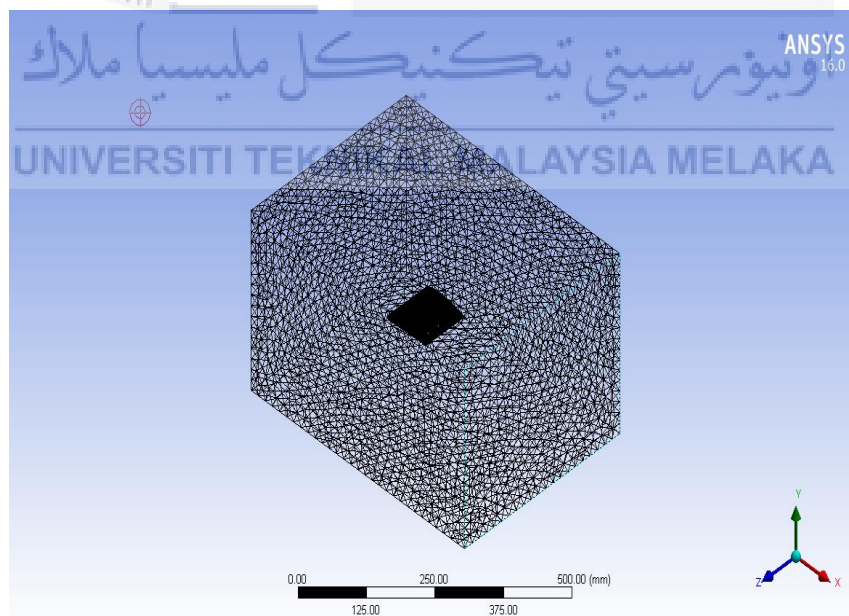


Figure 3.7: Meshing done airfoil and the fluid domain

3.4 Setup for Simulations

The assumption made for the simulation are as follow; steady state flow, turbulent flow. There are two different model used to simulate the CFD simulation which are S-A and SST models. In each model, two different airfoils are simulated at three different air velocity and different angle of attack. Air at 25°C is chosen as the fluid at the domain while the airfoil material is set to ABS. SIMPLE was chosen as the scheme for the pressure-velocity coupling at the solution method. SIMPLE is one of the Scheme which commonly used for CFD simulation. Least Square Cell Based was chosen for the gradient of the spatial discretization which can simulate more accurate compare to the other gradient of spatial discretization. Hybrid initialization was used to initialize the solution before running the calculation.

3.5 Post-Processing

In post-processing, the results for lift and drag force can be obtained. The lift and drag forces can be obtained by going to Report in Solution and select Forces under it. There are options in the Force report that the user needs to select. As for this project, the option would be force on the airfoil. Then set the direction vector to 1 on X direction to obtain the drag force or 1 on Y direction to obtain the lift force acting on the airfoil. The drag and lift forces also can be obtained when scrolling to the left where the total force acting the airfoil are list in X, Y and Z direction. Take the value of x and y for drag and lift force respectively as highlighted in Figure 3.8 and 3.9.

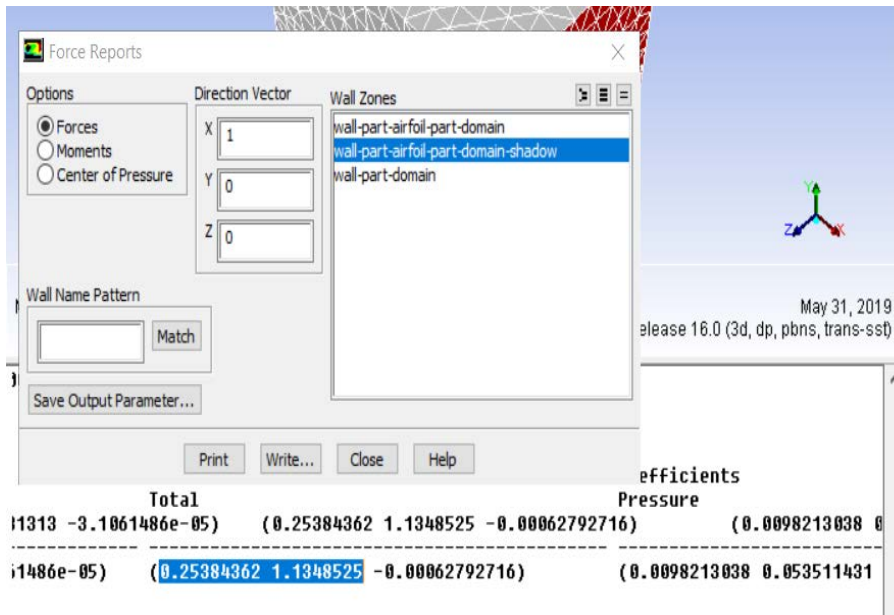


Figure 3.7: Aerodynamic forces on NACA 4418 at air velocity of 20 m/s and angle of attack of 10° using Transition SST model

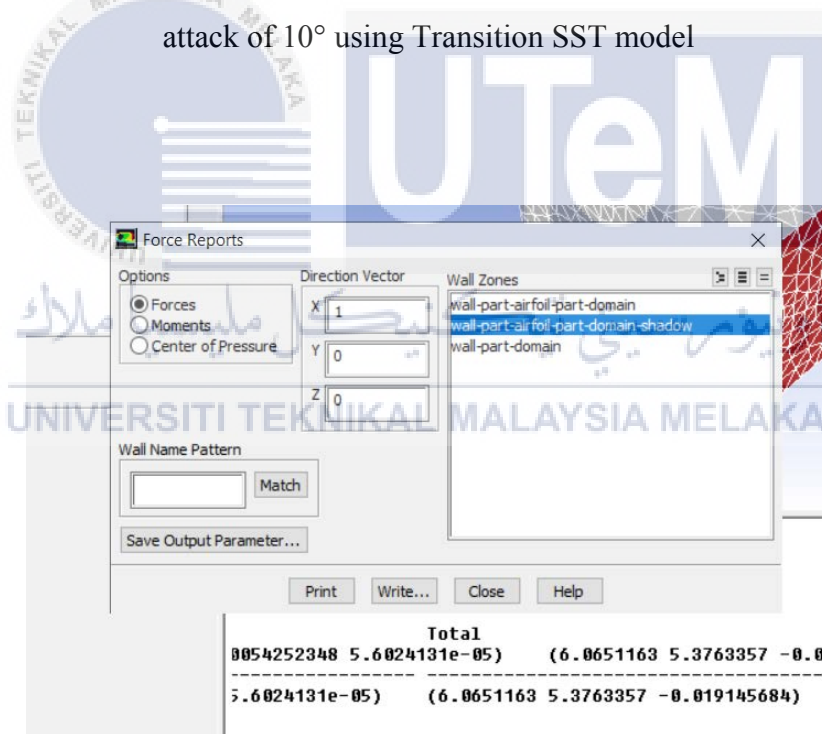


Figure 3.8: Aerodynamic forces on NACA 4412 at air velocity of 30 m/s and angle of attack of 50° using S-A model

CHAPTER 4

RESULTS AND DISCUSSION

4.0 Introduction

All the data obtained from the simulation of NACA 4412 and NACA 4418 using S-A and Transition SST at different air velocity and angle of attack are tabulated in form of table for easy excess of data. All the data are shown Appendix D and Appendix E. The lift and drag forces of both airfoils are compared at the different air speed and different turbulence models. The aerodynamic forces are analyzed and discussed for better understanding of the characteristic of each airfoil. The best angle of attack of each airfoil at different air velocity also obtained in this section.

4.1 Aerodynamic Forces Analysis on NACA 4412 and NACA 4418

The lift and drag forces for NACA 4412 and NACA 4418 are analyzed and discussed to see the stall angle, best angle of attack, maximum lift force on airfoil and comparison of forces at different air velocity. The lift and drag forces of NACA 4412 from the simulation using S-A model are tabulated in Table D.1 to D3 in Appendix D while the data of simulation by using Transition SST model are compiled in Table D.4 to D6 in Appendix D. The lift and drag forces from the simulation with S-A model for NACA 4418 are listed in Table E.1 to E.2 in Appendix E. Table E.4 to E.6 in Appendix E. are the compilation of the lift and drag forces acquire from simulation using Transition SST model as the turbulent model.

4.1.1 Lift Force on NACA 4412

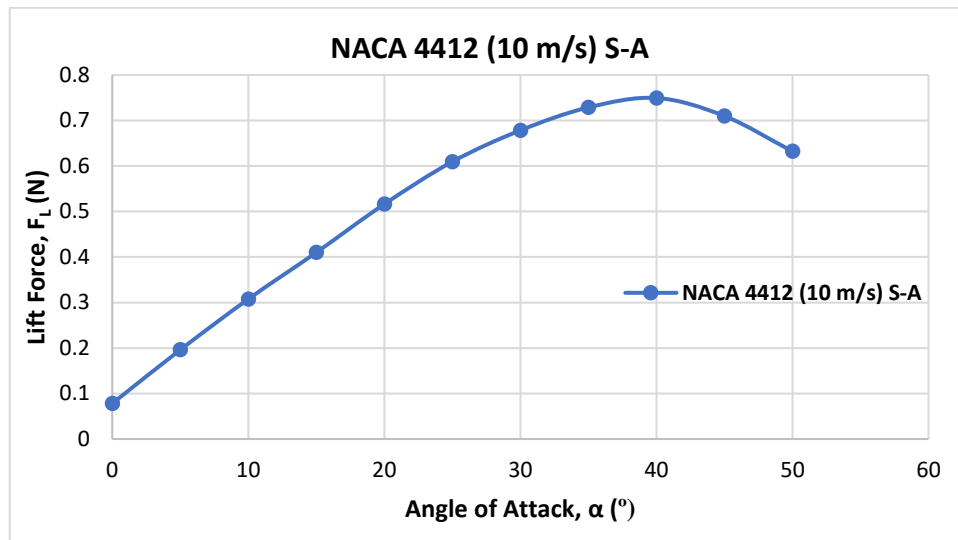


Figure 4.1: Graph of lift force of NACA 4412 using S-A model against different angle of attack at 10 m/s

Figure 4.1 shows the graph of lift force at different angle of attack at the air velocity of 10 m/s and simulated by using S-A turbulence model. The lift force increased from 0° until it reaches angle of 40° where the lift force values began to drop. This mean that the airfoil reaches critical stall angle at 40° for air velocity of 10 m/s. It reaches the stall angle because flow separation occurs on the upper surface of airfoil that prevent the airfoil to create more lift force. The highest value of lift force is at the stall angle, 0.74947 while the lowest value is at 0° with value of 0.07722. Based on the figure, the best angle of attack for the airfoil would be below 40° but above 35° to obtain the best lift force to lift the airfoil up for the air speed of 10 m/s. The angle needs to be less than 40° because it is the stall angle where the maximum lift force generated before the value drop. For NACA 4412 at 20 m/s and 30 m/s, the trend of the graphs is quite similar but the stall angle is different. This will be discussed more when comparing the different velocities later.

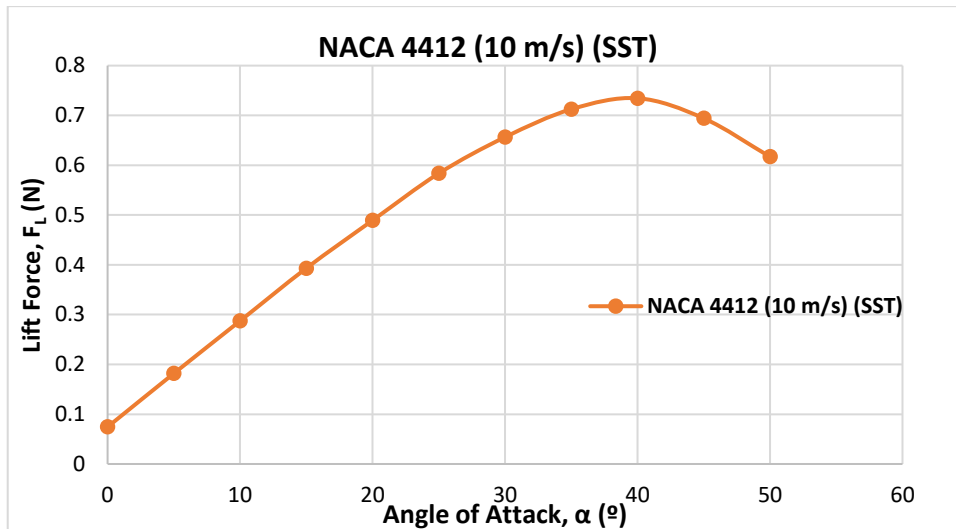


Figure 4.2: Graph of lift force of NACA 4412 using SST model against different angle of attack at 10 m/s

Figure 4.2 shows the graph of lift force at different angle of attack at air velocity of 10 m/s and simulated by using Transition SST turbulence model. The value of lift force increasing from 0° until 40° then it is decreasing from that point onward. Air flow separation occur after 40° which can stalling happen on the airfoil where not enough lift force generated to lift the airfoil up again. The highest value of lift force is at the stall angle, 0.07446 while the lowest value is at 0° with value of 0.02086. The best angle of attack for the airfoil would be below 40° but above 35° to obtain the maximum lift force at the air speed of 10 m/s.

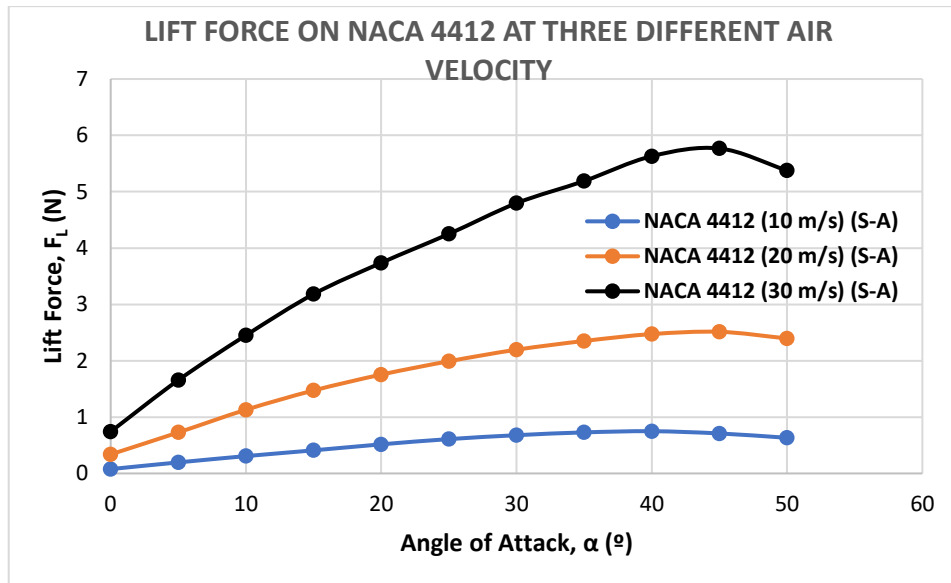


Figure 4.3: Graph of lift force of NACA 4412 against different angle of attack for S-A

Model

Figure 4.3 presents the lift force acting on NACA 4412 at three different speed and various angle of attack that were simulated using S-A model in ANSYS FLUENT 16. The results show that the higher the speed of air, the higher the lift force can be generated by the airfoil at angle of attack below the stalling angle. The reason for this is stated in Bernoulli's principle where increase in fluid's speed causes the decrease in pressure so that the energy is conserve. The shape of airfoil plays the important roles here because due to the shape, the air flow faster on upper surface compare to the lower surface of the airfoil.

Therefore, cause the pressure on the upper surface to drop while the lower surface has higher pressure. The high pressure on the lower surface will push the airfoil up and thus, creating what known as lift force. Noted that the stall angle for air velocity of 10 m/s is at 40° while the others are at 45°. The lift force after stalling is higher at 30 m/s compare to the other two air velocity.

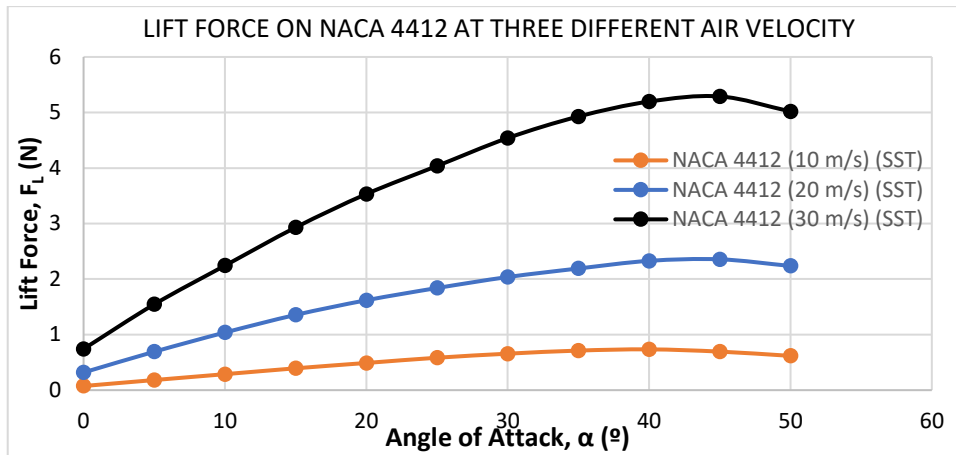


Figure 4.4: Graph of lift force of NACA 4412 against different angle of attack for Transition SST Model

Figure 4.4 illustrates the lift force acting on NACA 4412 at three different speed and various angle of attack simulated using Transition SST model. It is shown that increased in speed of air past through the airfoil lead to increase in lift force as well at angle of attack below stall angle. The trend is similar to forces generated using S-A model but differ in values. the stall angle for air velocity of 10 m/s is at 40° while the others are at 45°.

4.1.2 Drag Force on NACA 4412

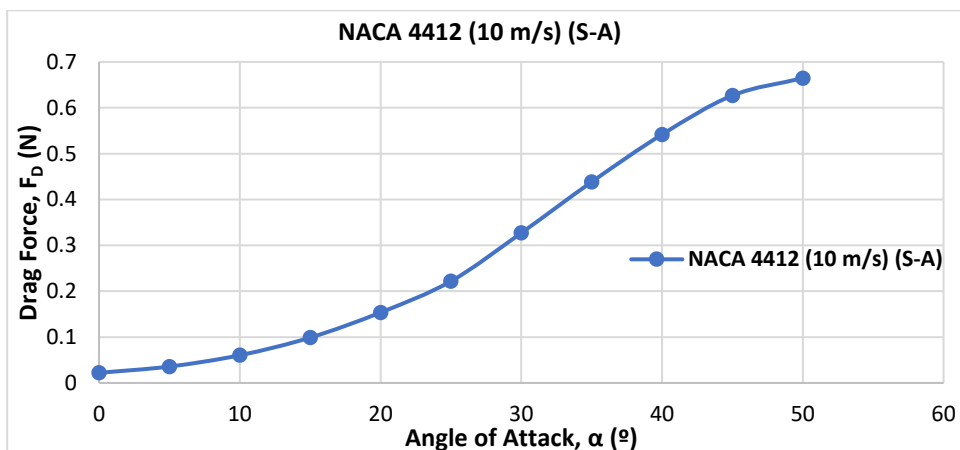


Figure 4.5: Graph of drag force of NACA 4412 using S-A model against different angle of attack at 10 m/s

The drag forces at the three different speed that were simulated by using S-A model are represented in the graph of Figure 4.5. From the graph, it is clearly shown that the drag forces acting on the NACA 4412 airfoil are increase as the air velocity that flow around the airfoil are increase. This is due to skin friction drag which cause by shear stresses on the surfaces of the airfoil. The internal stresses are produces because of the velocity gradient throughout the boundary layer of the airfoil. Thus, increase in velocity lead increase in skin friction drag on surface of the airfoil. Besides, as velocity and angle of attack increase, flow separation occurs where air becomes detaches from the surface of the wing. As this occur, the pressure on trailing edge will drop and reverse flow will occur. Thus, it will increase the pressure drag acting on the airfoil.

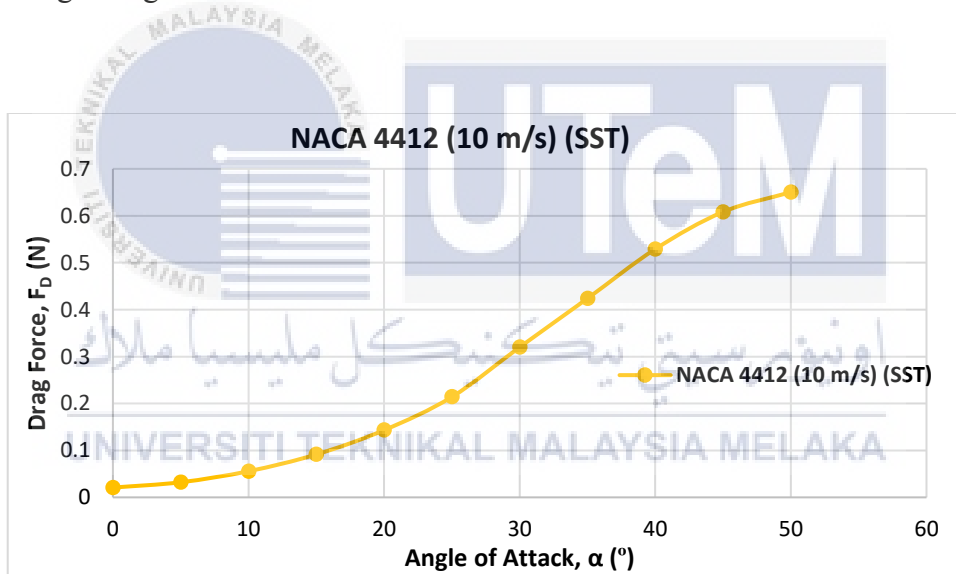


Figure 4.6: Graph of drag force of NACA 4412 using Transition SST model against different angle of attack at 10 m/s

Figure 4.6 displays the drag forces for NACA 4412 at angle of attack ranging from 0° to 50° at air velocity of 10 m/s. The value for drag keeps elevate until the end of angle of attack simulated due to increasing in pressure different between the leading edge surface to the trailing edge surface cause increase in pressure drag. The highest value for drag force is 0.65037 while the lowest value is 0.02086.

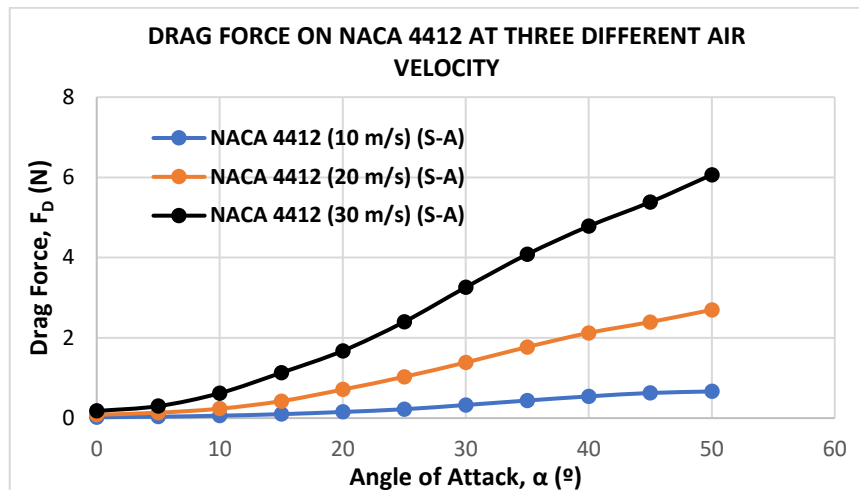


Figure 4.7: Graph of drag force of NACA 4412 against at three different speed and angle of attack for S-A model

The drag forces at the three different speed that were simulated by using S-A model are represented in the graph of Figure 4.7. The drag forces acting on the NACA 4412 airfoil are increase as the air velocity that flow around the airfoil are increase. This is because skin friction drag and pressure drag cause the increase in total drag force when the air velocity flow around the airflow increase.

Figure 4.8 shows the drag forces at three different air velocity that were simulated by using Transition SST model. The drag force on airfoil increase with the increase of air velocity because the friction between air and the surface of the airfoil create skin friction drag. Besides, the increase in different of pressure different in the front area and the rear area cause increase in pressure drag as well.

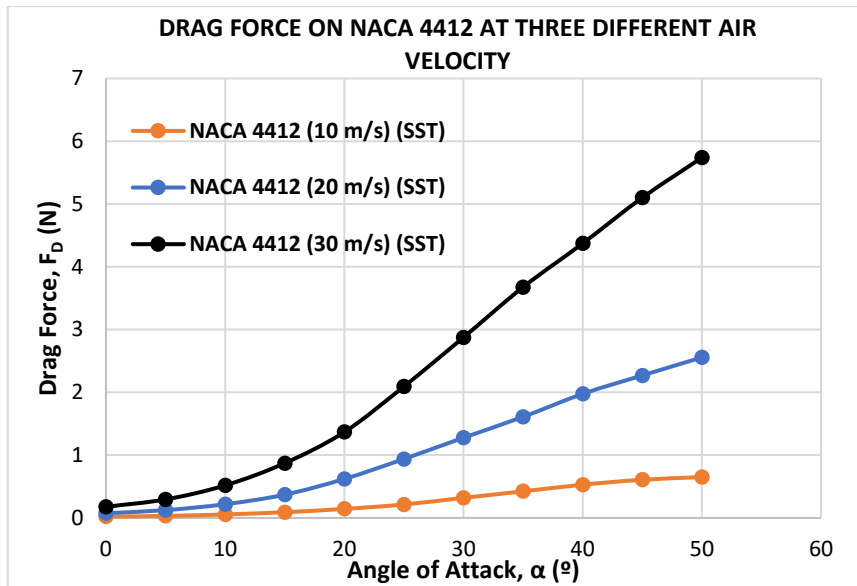


Figure 4.8: Graph of drag force of NACA 4412 against at three different speed and angle

of attack for Transition SST model

4.1.3 Lift Force on NACA 4418

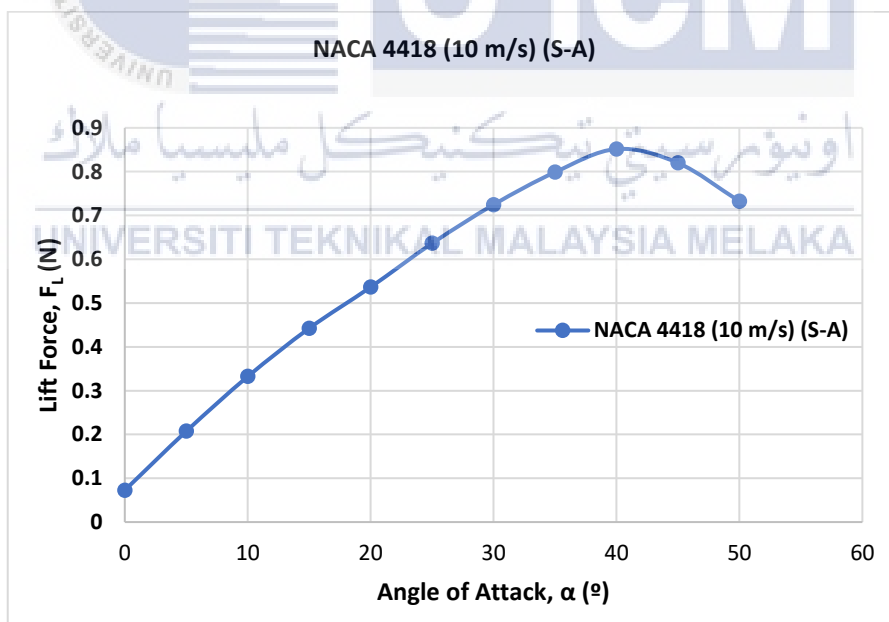


Figure 4.9: Graph of lift force of NACA 4418 using S-A model against different angle of attack at 10 m/s

The lift force at velocity of 10 m/s is increasing from 0° until it reaches the stall angle of 40° which is displays in the graph of Figure 4.9. Larger flow separation in the upper surface of the airfoil lead to decreasing in lift force after the stall angle. The peak value of lift force from the graph is 0.85164 while the lowest value is 0.07269. It best to avoid the stall angle because increase in angle of attack can lead to stalling to happen. Thus, the best angle of attack for the airfoil at 10 m/s ranging between below 35° to below 40° for higher lift force to lift the airfoil.

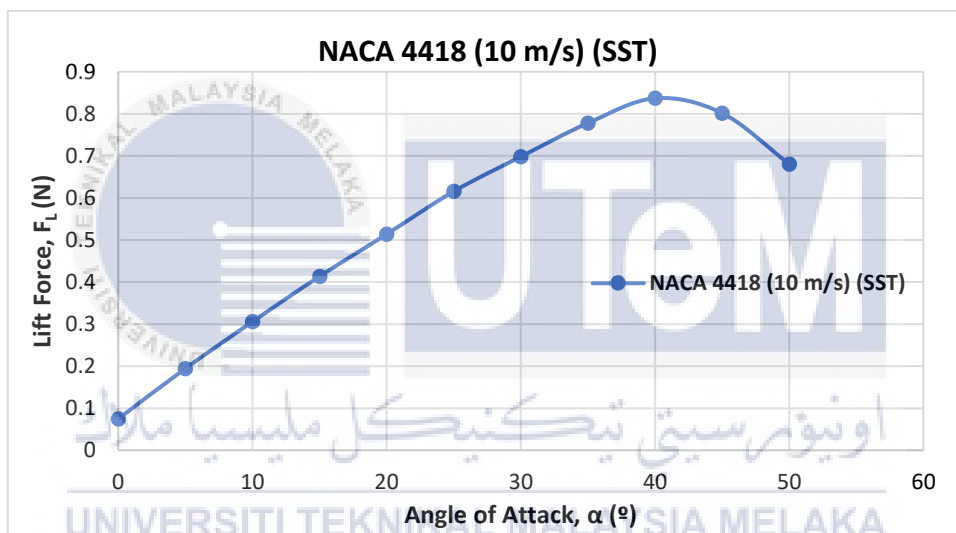


Figure 4.10: Graph of lift force of NACA 4418 using Transition SST model against different angle of attack at 10 m/s

The trend of graph for NACA 4418 using Transition SST model in Figure 4.10 is similar to previous graph where the lift force increases as the angle of attack until it reaches the stall angle of 40° where the lift force decreases after that point. The maximum lift that NACA 4418 able to produce is 0.83699 while the minimum force it produces as shown in graph is at 0° with the value of 0.07476.

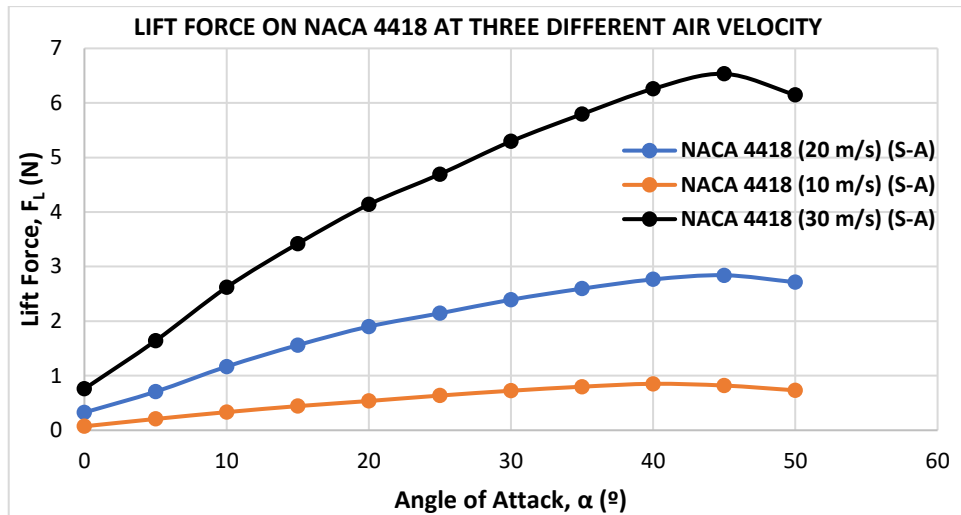


Figure 4.11: Graph of lift force of NACA 4418 against different angle of attack for S-A Model

Figure 4.11 shows the lift force acting on NACA 4418 at three different speed and various angle of attack simulated using S-A model in ANSYS FLUENT. As the air speed pass through the airfoil increase, the lift force acting on the airfoil also increase. This is shown in the graph as the gap between each line are increase. This is due to increase in fluid velocity causes the decrease in pressure as stated in Bernoulli's Principle. The air flow faster on upper surface compare to the lower surface of the airfoil due to the streamline shape.

Therefore, the pressure on the upper surface to drop while the lower surface has higher pressure. Lift force is generated as the high pressure on the lower surface will push the airfoil up. Besides, lift force relationship also can be seen in equation 2.5 where the lift force increases with velocity in the mathematical model.

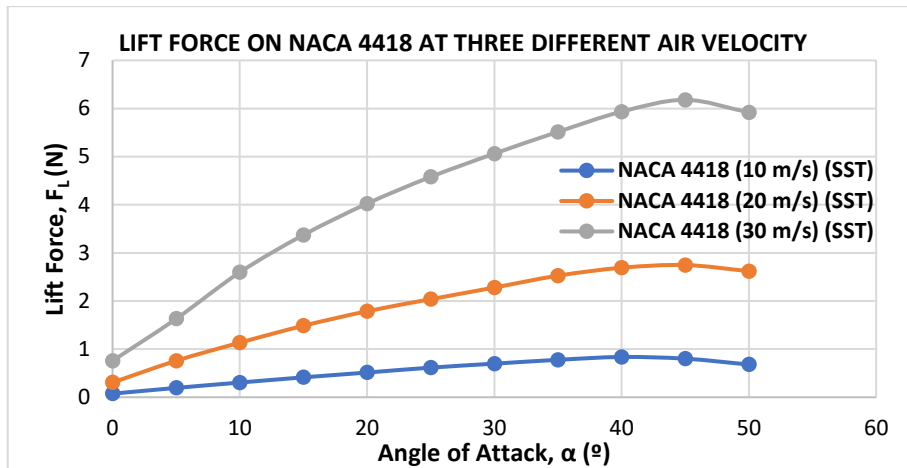


Figure 4.12: Graph of lift force of NACA 4418 against different angle of attack for Transition SST Model

Figure 4.12 illustrates the lift force acting on NACA 4418 at three different speed and various angle of attack simulated using Transition SST model. From the figure, increase in speed of air past through the airfoil lead to increase in lift force as well at angle of attack below stall angle. The trend is similar to forces generated using S-A model but differ in values because of different type of turbulence model.

UNIVERSITI TEKNIKAL MALAYSIA MELAKA

4.1.4 Drag Force on NACA 4418

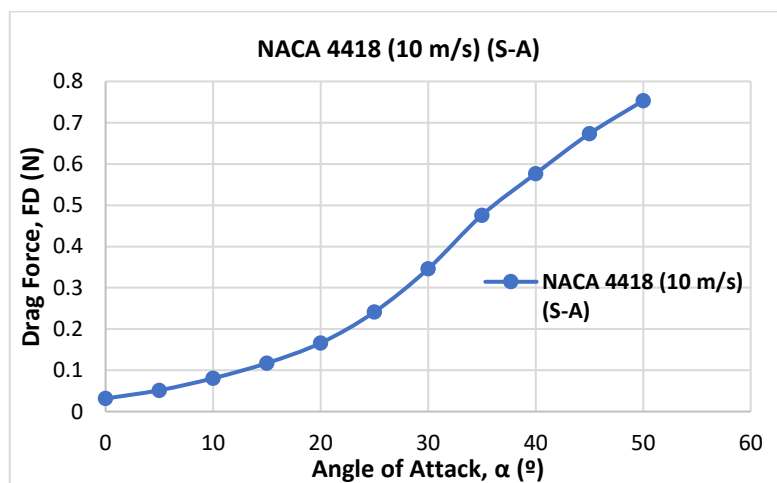


Figure 4.13: Graph of drag force of NACA 4418 using S-A model against different angle of attack at 10 m/s

Figure 4.13 shows the drag force for NACA 4418 is increase as the angle of attack increases. The trend of the graph for drag force against different angle of attack at 10 m/s is similar with the trend of drag force graph for the other two air velocity. The highest value for coefficient of drag is at 50° whereas the lowest value is at 0° with the value of 0.75329 and 0.03156 respectively. Reverse flow will occur especially at angle of attack after the stall angle. Thus, it will increase the pressure drag acting on the airfoil.

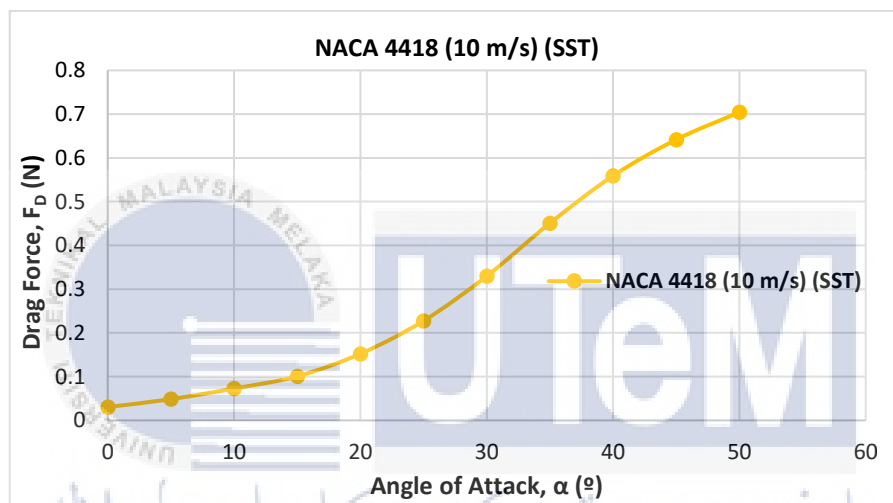


Figure 4.14: Graph of drag force of NACA 4418 using Transition SST model against different angle of attack at 10 m/s

The coefficient of drag for NACA 4418 is increase as the angle of attack increases as shown in Figure 4.14. The trend of the graph for drag coefficient against different angle of attack at 30 m/s is similar with the trend at air velocity of 10 m/s and 20 m/s with different values. The highest value for coefficient of drag is at 50° whereas the lowest value is at 0° with the value of 0.70434 and 0.03049 respectively.

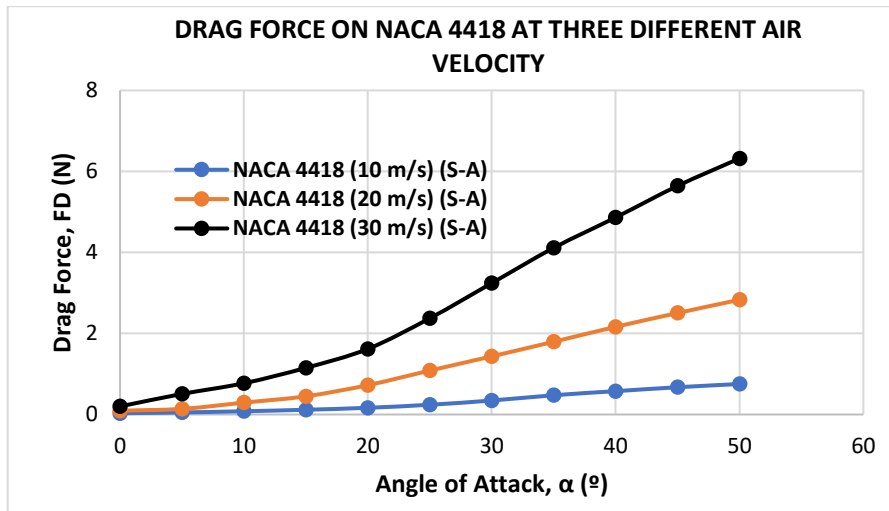


Figure 4.15: Graph of drag force of NACA 4418 using S-A model at three different air velocity

The drag forces at the three different speed that were simulated by using S-A model are represented in the graph of Figure 4.15. The drag forces acting on the NACA 8441 airfoil are increase as the air velocity that flow around the airfoil are increase because of skin friction drag and pressure drag. Increase in air speed caused air flow detached from the surface of the airfoil which cause increase in drag pressure

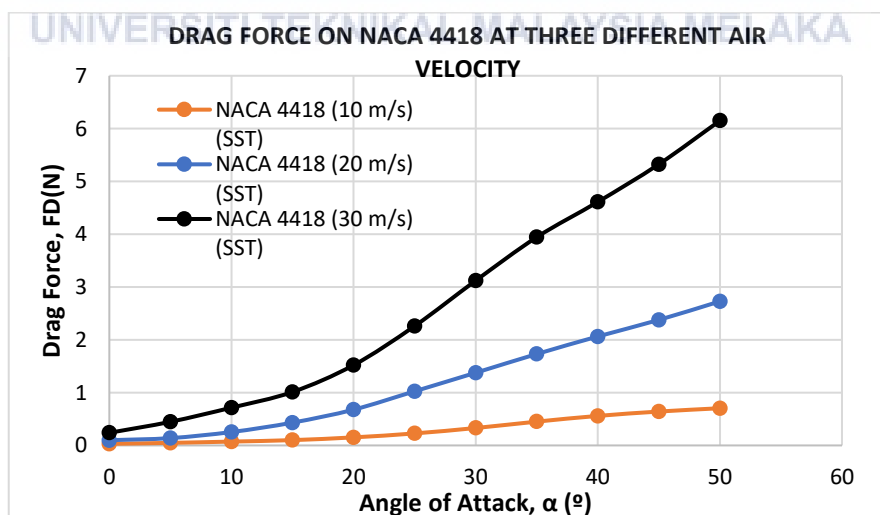


Figure 4.16: Graph of drag force of NACA 4418 using Transition SST model at three different air velocity

The drag forces at the three different speed that were simulated by using SST model are represented in the graph of Figure 4.16. As the angle of attack increase and becoming steeper, the separation point toward the trailing which lead to increase in pressure drag.

4.2 Comparison Between Results Obtained From S-A Model and Transition SST Model for NACA 4412

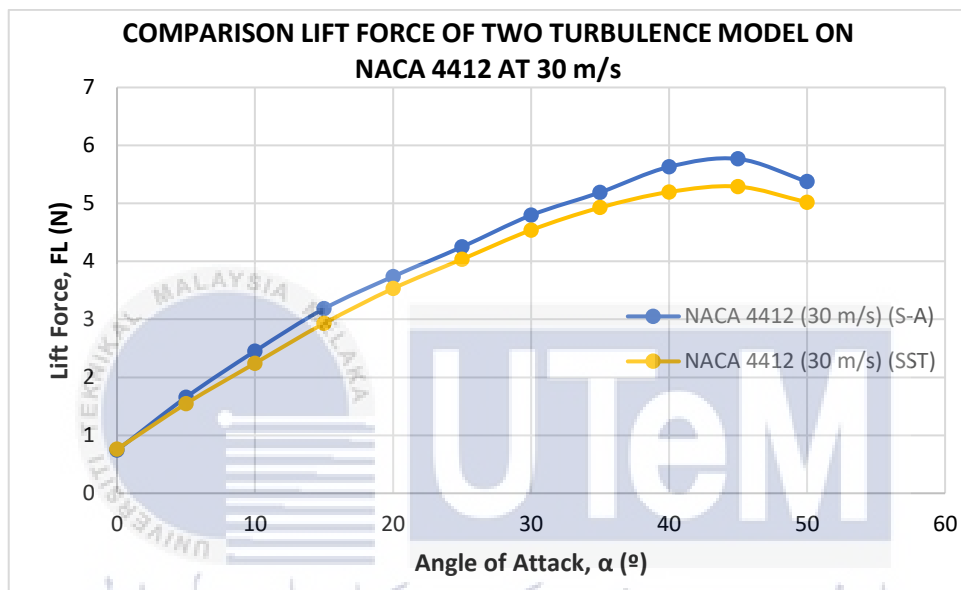


Figure 4.17: Graph of lift force against different angle of attack for S-A and Transition SST Model

Figure 4.17 shows the comparison between lift force that produce in simulation by using S-A and Transition SST model. The values of lift force for S-A model are slightly higher compare to lift force that simulated using SST model from 20° whereas the value before that are nearly identical. From previous study, most of the results obtained for S-A model are higher compare to SST model.

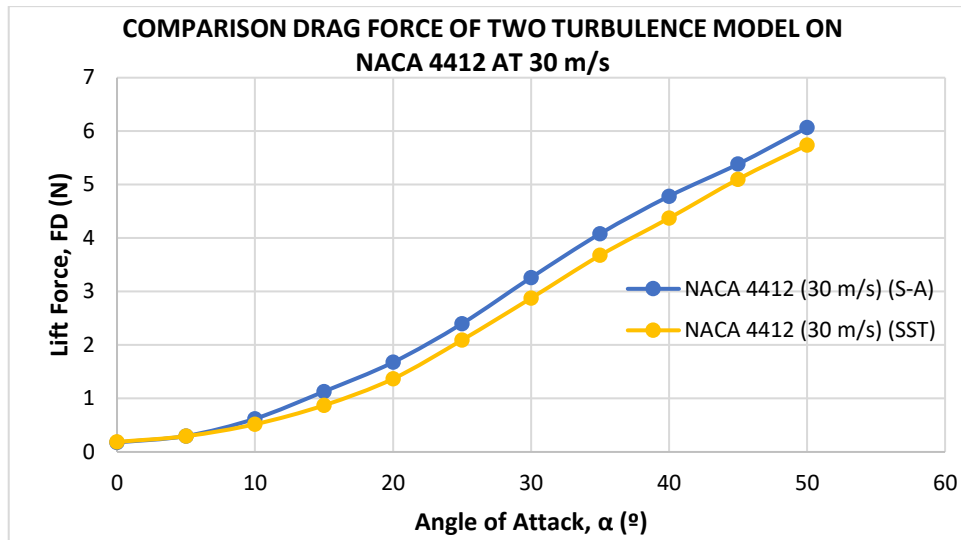


Figure 4.18: Graph of drag force against different angle of attack for S-A and Transition

SST Model

Figure 4.18 shows the comparison between drag force that produce in simulation by using S-A and Transition SST model. The values of drag force for S-A model are greater than Transition SST model from 10° to 35°.

4.3 Comparison Between Results Obtained From S-A Model and Transition SST Model for NACA 4418

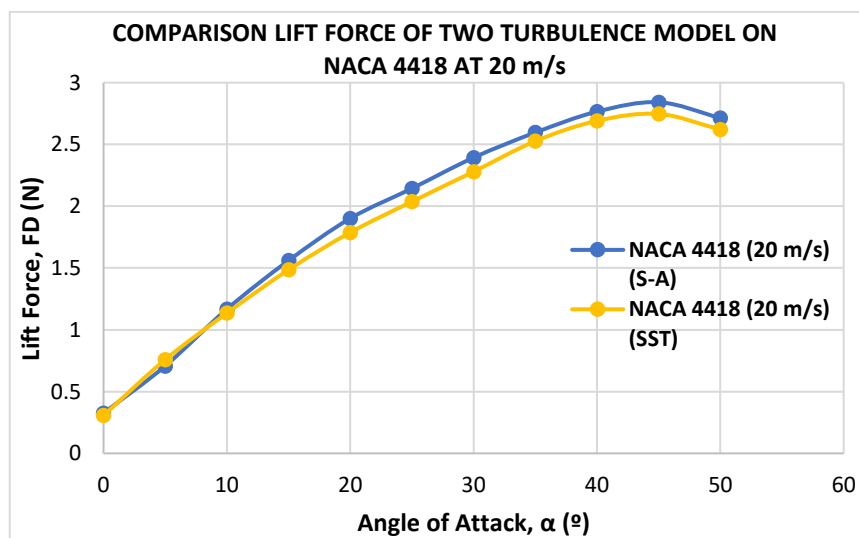


Figure 4.19: Graph of lift force against different angle of attack for S-A and SST Model

Figure 4.19 shows the comparison between lift force that produce in simulation by using S-A and Transition SST model. The values of lift force for S-A model are slightly higher compare to lift force that simulated using Transition SST model at the value after 35° whereas the value before that are nearly identical.

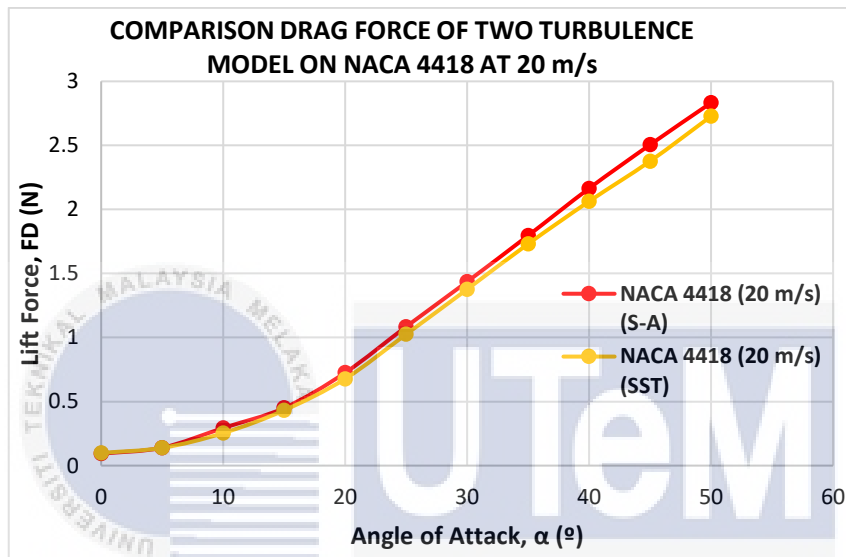


Figure 4.20: Graph of drag force against different angle of attack for S-A and SST Model

Figure 4.20 shows the comparison between drag force that produce in simulation by using S-A and Transition SST model where values of drag force for S-A model are nearly the same as Transition SST model from 0° to 30° but the value increase compare to drag force that simulated using SST model.

4.4 Aerodynamic Forces Comparison Between NACA 4412 and NACA 4418

Lift and drag force obtained from simulation of NACA 4412 and NACA 4418 using SST turbulent model at 30 m/s are compared to see the effect of maximum thickness of

airfoil to the aerodynamic forces acting on airfoil. NACA 4418 has higher maximum thickness than NACA 4412.

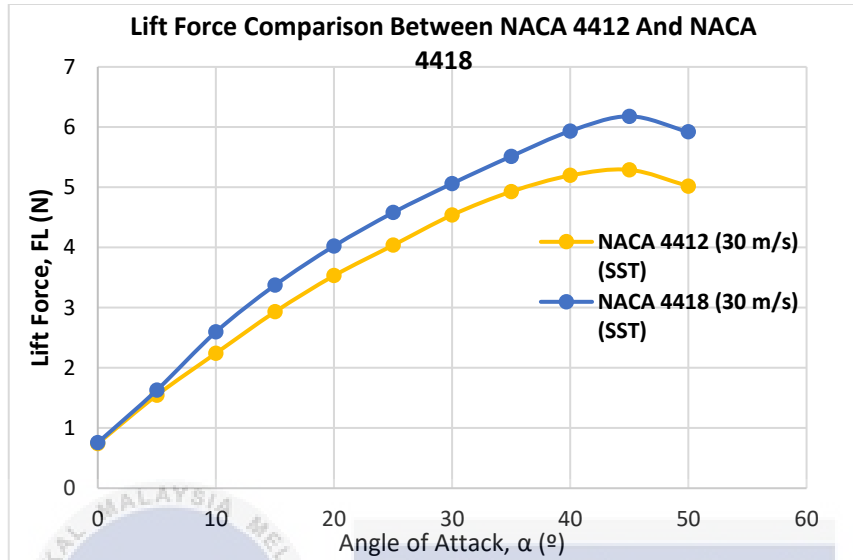


Figure 4.21: Graph of lift force against angle of attack at 30 m/s between NACA 4412 and NACA 4418

From Figure 4.21, the lift force for both airfoils are almost similar from angle of attack of 0° to 5°. The lift force for NACA 4418 are higher compare to NACA 4412 from the angle of 5° to 50°. Both airfoils have the same stall which is at 45° but the maximum lift force for NACA 4418 is 6.17942 while the maximum lift force for NACA 4412 is 5.2898. NACA 4418 produce higher maximum lift force compare to NACA 4412 due to the maximum thickness. NACA 4418 has thicker maximum thickness compare to NACA 4412 where the geometry plays important roles in increasing lift force of the airfoil. The best angle of attack for NACA 4418 and NACA 4412 are ranging between 40° to below 45° where after the critical angle of attack stalling occur.

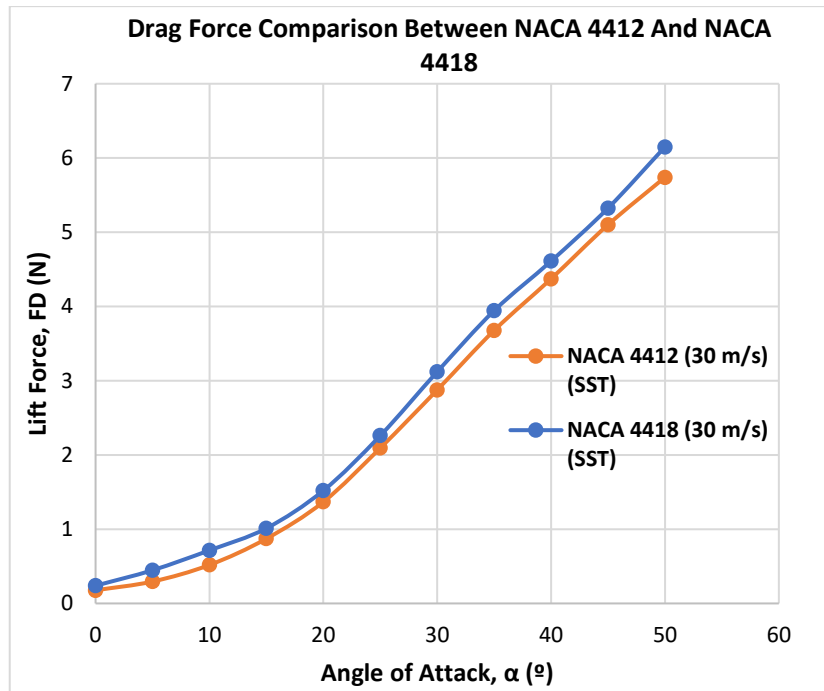


Figure 4.22: Graph of drag force against angle of attack at 30 m/s between NACA 4412 and NACA 4418

Figure 4.22 shows the drag force generated by both airfoils at air velocity of 30 m/s at angle of attack from 0° to 50° by using SST turbulence model. The trend for the graph is same for both airfoil where both increase until reaching 50° . As shown in graph, NACA 4418 generate more drag force compare to NACA 4412. Increase in maximum thickness does affect the lift and drag force of an airfoil. It will increase the maximum lift force generated by the airfoil as portrayed by NACA 4418 in Figure 2.1.

4.5 Visualization of Simulated Airfoils Using Contours

These are example contours that can be generated in ANSYS FLUENT. These contours represent the pressure and velocity distribution acting on and around the airfoil. The colours in the contour represent values that indicated on the scale on the contours.

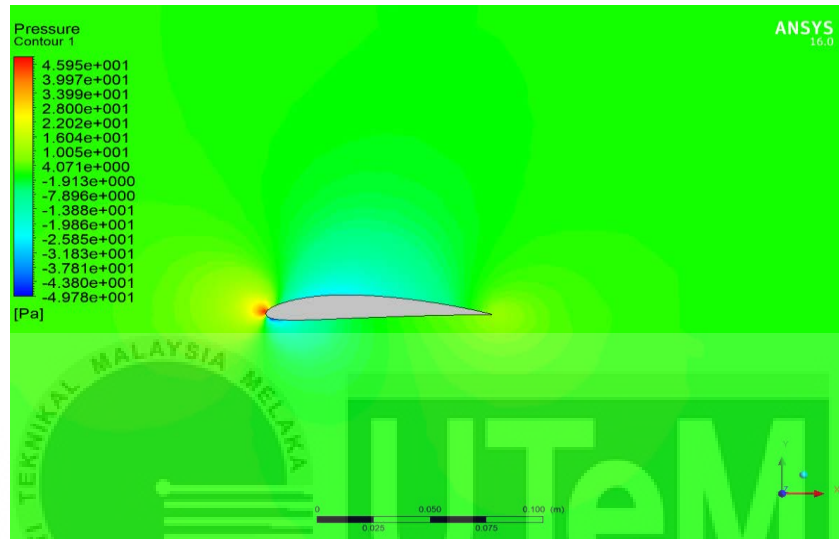


Figure 4.23: Pressure contour at angle of attack, 0°

Figure 4.23 show the pressure contour on NACA 4412 airfoils that simulated using Transition SST model at air velocity of 10 m/s. The contour indicates that the pressure on upper surface of the airfoil are lower than the lower surface of the airfoil. This is indicated by light blue colour on top surface while yellowish-green on the bottom surface. The upper surface has lower pressure because the air flow on top surface is faster compare to the lower surface as shown in velocity contour in Figure 4.24. On top surface the it has red mix with orange color which indicate the higher speed compare to the lower part of airfoil which colour are yellow mix with a little bit of orange. As velocity increase the pressure decrease according to Bernoulli's Principle. Thus, lift force are able to be created.

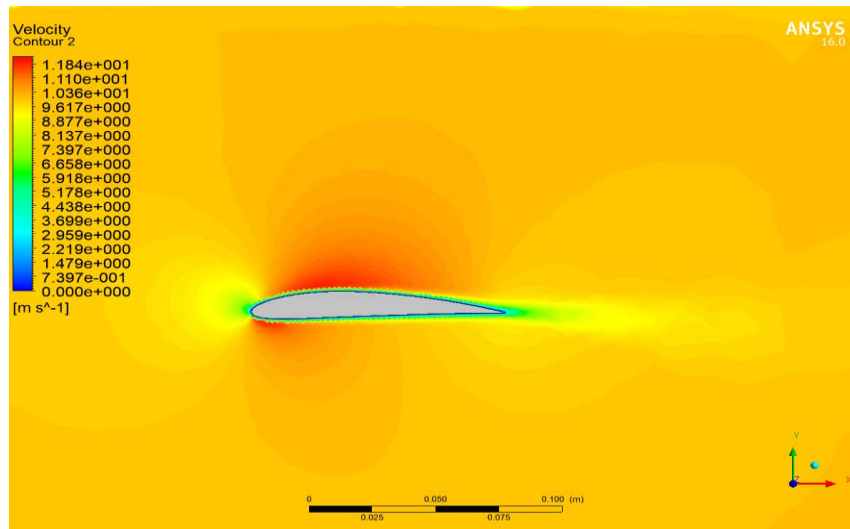


Figure 4.24: Velocity contour at angle of attack, 0°

On the trailing edge or rear of the airfoil, it can be seen that the velocity is lower compare to the leading edge as shown in Figure 4.24. This velocity affects the pressure on both edges as well where there is pressure different between the leading and trailing edge as shown pressure contour in Figure 4.23. Different in pressure on leading edge and trailing edge cause increasing in pressure drag. Figure 4.25 shows the direction of air flow acting on the airfoil. As shown in figure, there is no vortex created on the trailing edge of the airfoil.

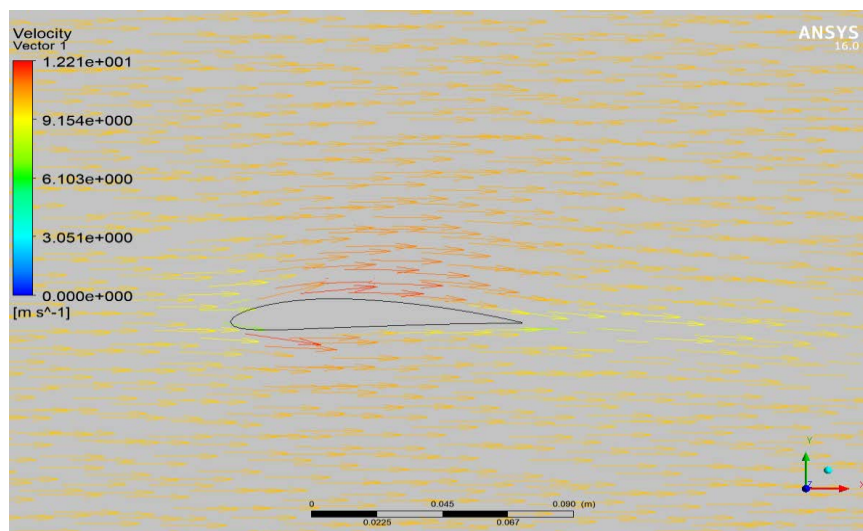


Figure 4.25: Velocity vector at angle of attack, 0°

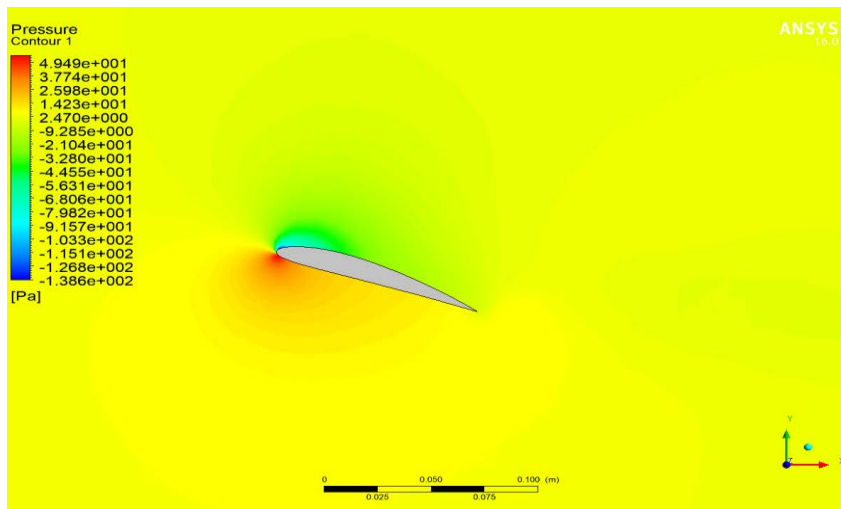


Figure 4.26: Pressure contour at angle of attack, 20°

Figure 4.26 shows the pressure contour of NACA 4412 airfoil as the angle of attack increased to 20° and simulated same as the previous contours. As shown in the contour, the pressure different acting on the airfoil increased as the angle of attack increased. The top surface has green mix with light blue colour whereas orange and yellow colour on bottom surface. This is because the angle makes the air flow faster on top surface as shown in Figure 4.27. as the pressure different increase, the lift force generated is increased as well.

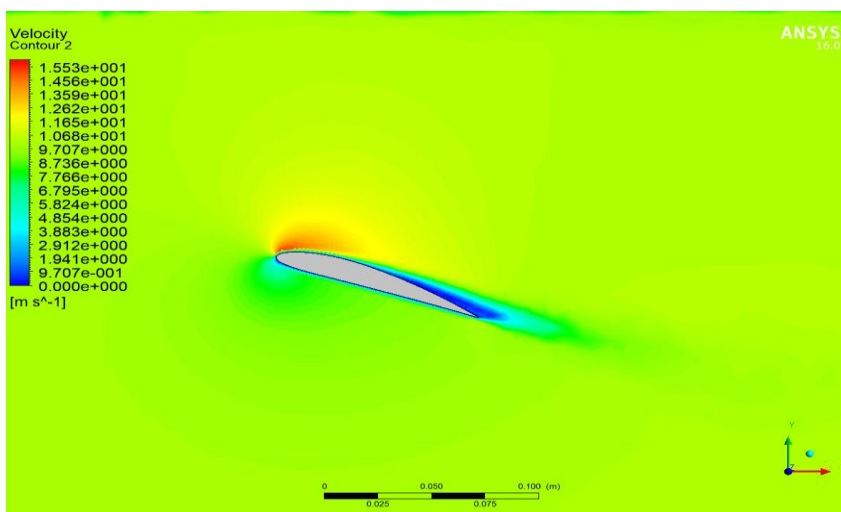


Figure 4.27: Velocity contour at angle of attack, 20°

The flow began to separate from the trailing edge as the angle of attack increased as can be seen in trailing edge of velocity contour and velocity vector in Figure 4.27 and Figure 4.28 respectively. The flow become detached from the trailing edge and less flow indicated by the arrow in velocity vector on the trailing edge. Increased in pressure on trailing edge also increase the pressure drag and push the airfoil downward causing reduce in lift.



Figure 4.28: Velocity vector at angle of attack, 20°

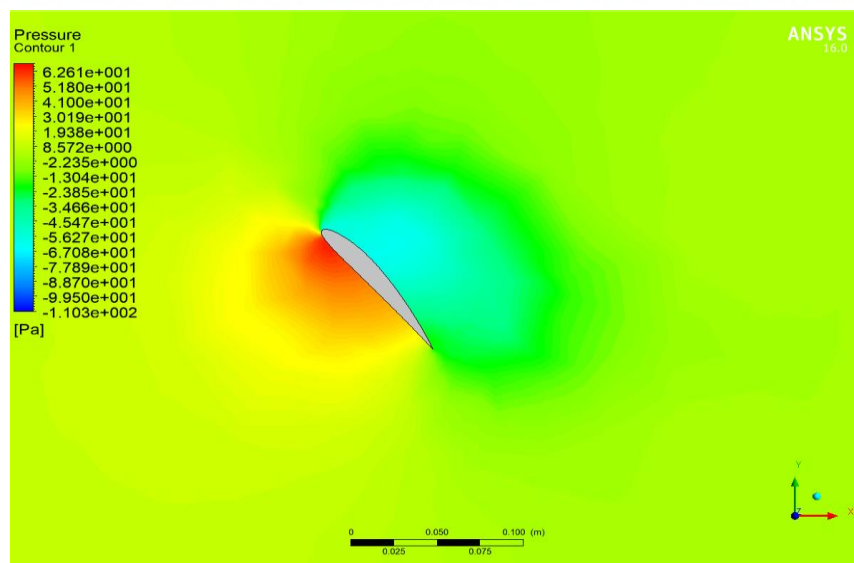


Figure 4.29: Pressure contour at angle of attack, 50°

The pressure on top of the surface are much lower compare to the lower surface of the airfoil as shown in Figure 4.29. It supposed to increased the generation of lift force since the different of pressure on top and lower are significant but less lift force is produced due to the pressure different on leading edge and trailing edge create more drag force on the airfoil. The lower pressure on the trailing edge also indicate that flow separation happened. As shown in Figure 4.30, the separation that occur is indicated by the bright blue colour that indicate zero air flow on that are. Flow separation become bigger compare to when the angle of attack at 20° on the trailing edge.



Figure 4.30: Velocity contour at angle of attack, 50°

The separation of air flow also created eddies and vortices on the trailing edge of the airfoil as shown in Figure 4.30. Reverse flow occurs as indicated by the arrow where it flows back on the airfoil instead of flowing past through it. Vortices will create more skin drag on the upper surface while the flow separation increase the pressure drag. Increase in drag will lower the lift force. Thus, stalling happened as the lift force unable to lift up the airfoil anymore.

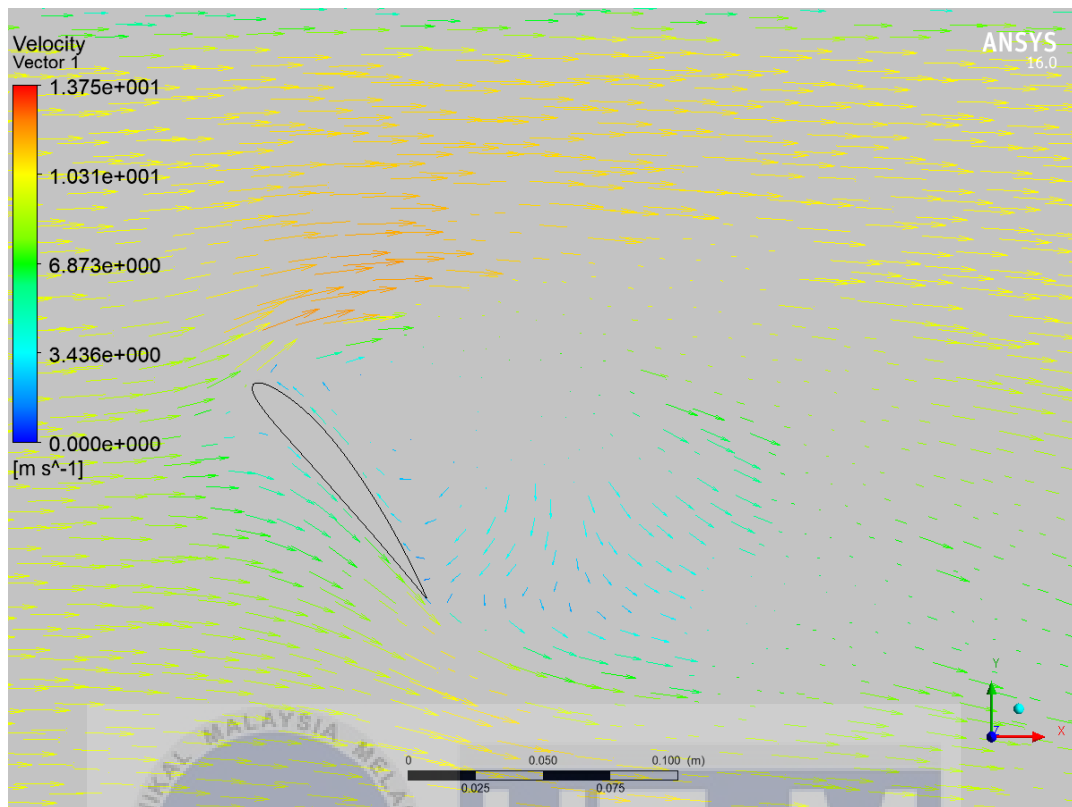


Figure 4.31: Velocity vector at angle of attack, 50°

As shown in Figure 4.31, the air flow become totally detached from the trailing of the airfoil and reverse flow occur as well that created vortex which increase the drag on the trailing causing not enough lift generated to lift the airfoil up.

4.6 Validation of Data

The results obtain from the simulation need to be validated in order to prove it accuracy. On early stage of this project, the results were supposedly validated by doing experiment in wind tunnel but due to technical problem which cause the wind tunnel unable to be used. Therefore, the results will be validated with the results obtained from past study on the airfoil.

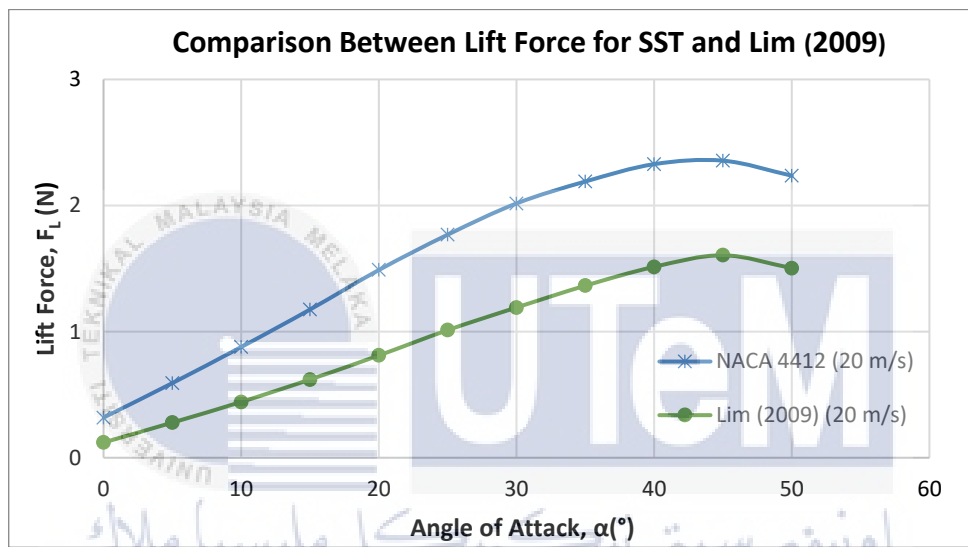


Figure 4.32: Comparison between lift force obtained through simulation with Lim (2009)

Figure 4.32 shows the lift forces obtained by Lim (2009) and the result simulated in for this project. There are clear different in the values obtained for the lift force on current simulation compare to Lim (2019) but both have the same trend of graph where lift force on both simulations increase until reaching stall angle of 45° then the value began decreasing. There is some reason for the different in value obtained. Both were simulated using Transition SST model at the same airfoil, air speed and chord length. The different is the results for Lim (2009) were simulated using ANSYS CFX while the simulation in project is simulated with ANSYS FLUENT. Both FLUENT and CFX are almost identical but some interface on both software are a little bit different. For example, in ANSYS FLUENT, the

type of scheme and spatial discretization for the modelling needed to be chosen whereas there no setting for this in ANSYS CFX.

Besides, lack of details on the simulation make it harder to simulate exactly the same simulation and obtaining more accurate results. For example, details on how to set the velocity when there is angle of attack apply to the airfoil is not clearly clarified on the journal. Furthermore, details on how to obtain the results for lift and drag forces at different angle also did not clearly stated but the journal state that the lift force obtain through post-processing result where lift is in y-direction while drag is in x-direction in the force vector.

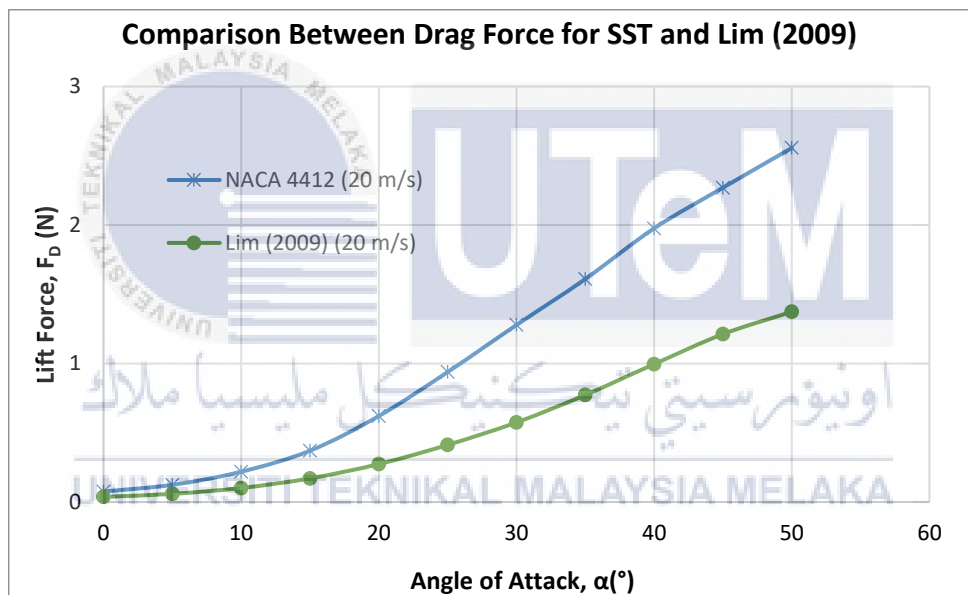


Figure 4.33: Comparison between drag force obtained through simulation with Lim (2009)

Figure 4.33 shows the different in drag force obtained for Lim (2009) and the simulation done for this project at 20 m/s for NACA 4412. The simulation in this project have higher drag compare to the simulation done by Lim (2009). Higher drag usually undesirable for airfoil. Lack of processing power in laptop also making it hard to simulate at finer mesh and more iterations for better results.

The comparison between results obtained from both simulations is not acceptable due to lack of accuracy in values obtained even though the pattern of the graph for lift and drag forces having quite similar pattern.



CHAPTER 5

CONCLUSION AND RECOMMENDATION

5.0 Conclusion

As a conclusion, CFD simulations on NACA 4412 and NACA 4418 were done by using Spalart-Allmaras and Transition Shear Stress Transport in ANSYS FLUENT 16 to obtain the aerodynamic forces acting on the airfoils. Air velocity of 10 m/s, 20 m/s and 30 m/s were used in the simulation while the angle of attack varies from 0° to 50° with increment of 5°.

Lift and drag force obtained from the simulations are tabulated in form of table and graph. From the result obtained, aerodynamic forces in simulations using S-A are slightly higher compare to results from simulation using Transition SST. As velocity increase the value for the aerodynamic forces also increase. The lift force increases for both airfoil from the initial angle of attack, 0° until both reach stall angle. The stall angle for both NACA 4412 and NACA 4418 is at 40° at 10 m/s while stall at 45° for the other two air velocity. NACA 4418 has higher maximum lift force compare to NACA 4412 due to effect of thickness on the aerodynamic force acting on airfoil where thicker airfoil has better aerodynamic force.

The best angle of attack to obtain high lift force for both airfoils at different velocities ranging from 35° to below 40° for air velocity of 10 m/s while the range for the other two air velocity are from 40° to below 45. It can be said that performance of NACA 4418 is better compare to NACA 4412 but there are other factors besides the aerodynamic forces determine which airfoil should be chosen for that application. Each airfoil is unique and

factors such as the intended speed range, maximum weight and size of application also needed to be considered when choosing the airfoil.

The results obtained are not entirely accurate compare to others results from past studies even though the meshing is already refined similar to the journal and mesh adaption are done after finishing the simulations. Due to time constraint and limit of computer power, the much finer meshing was not able to be done. The trend for the results still follows the results from past studies but its values are higher compare to the results of past studies.

5.1 Recommendation

There are other types of turbulence models in ANSYS such as k-epsilon, k-omega and others that can be used in CFD simulation especially for airfoil. Each type of turbulence models has their own advantage and disadvantages. Therefore, a proper research on those models are require. As for simulation of airfoil, consider a C-type meshing for the domain and make structural mesh around the airfoil for better meshing on the airfoil. There are also a lot more type of airfoil out there that used in various applications such frontal and rear wing of racing car and turbine's blade. Doing analysis on these airfoils may lead to better understanding on that certain airfoils.

REFERENCES

- E. Abrahams and D. Cladwell, 2005. McGraw-Hill Encyclopedia of Science and Technology, 6th Ed. (McGraw Hill, New York, NY,)
- Wikipedia. Airfoil. Retrieved from <https://en.wikipedia.org/wiki/Airfoil> [Accessed on 10 October 2018]
- Yemenici, O., 2014. An Experimental Study on the Aerodynamics of a Symmetrical Airfoil with Influence of Reynolds Number and Attack Angle, 97–99.
- Tuncay Kamas. 2009. 2D and 3D Assessment of Cambered and Symmetric Airfoils: *A Computational Fluid Dynamics Study*.
- Koppula, R., 2018. The Top 6 Technologies for Improving Aircraft Fuel Efficiency. Retrieved from <https://www.prescouter.com/2018/01/technologies-improving-aircraft-fuel-efficiency/> [Accessed on 10 October 2018]
- Haque, M. N., Ali, M., and Ara, I., 2015. Experimental investigation on the performance of NACA 4412 aerofoil with curved leading edge planform. In *Procedia Engineering* (Vol. 105, pp.232–240).
- Bansal, R. K., 2005. *A textbook of fluid mechanics*. Delhi: Laxmi Publication (P) LTD.
- Çengel, Y. A., & Cimbala, J. M. (2009). *Fluid mechanics: Fundamentals and applications*. Boston: McGraw-Hill Higher Education.
- Al-Kayiem, H. H., and Kartigesh, A. K., 2011. An investigation on the aerodynamic characteristics of 2-D airfiol in ground collision. *Journal of Engineering Science and Technology*, 6(3), pp.371–383.
- Fatehi, M., Nili-Ahmadabadi, M., Nematollahi, O., Minaiean, A., and Kim, K. C., 2019. Aerodynamic performance improvement of wind turbine blade by cavity shape optimization. *Renewable Energy*, 132, pp.773–785.

Wang, Y., Shen, S., Li, G., Huang, D., and Zheng, Z., 2018. Investigation on aerodynamic performance of vertical axis wind turbine with different series airfoil shapes. *Renewable Energy*, 126, pp.801-818.

Q., 2016. Do Spoilers Actually Make Cars Go Faster? Retrieved from <https://www.forbes.com/sites/quora/2016/09/30/do-spoilers-actually-make-cars-go-faster/#2f24ddc76144> [Accessed on 3 November 2018]

Durrer, S., 2016. Aerodynamics of race car wings: A CFD study (MSc thesis), pp.255.

D'souza, A. G., Concessao, J. I., and Quadros, J., 2015. Study of Aerofoil Design Parameters for Low Speed Wind Tunnel, 5(1), pp.47–54.

Srinivasa Rao, T., Mahapatra, T., & Chaitanya Mangavelli, S. (2018). Enhancement of Lift-Drag characteristics of NACA 0012. In *Materials Today: Proceedings*, 5, pp.5328–5337).

Kevadiya, M. and Vaidya, H., 2013. 2d Analysis of NACA 4412 Airfoil. *International Journal of Innovative Research in Science, Engineering and Technology*. 02. Pp.1686 -1691.

Airfoil database search (NACA 4 digit). Retrieved from [http://airfoiltools.com/search/index?m\[textSearch\]=&m\[maxCamber\]=&m\[minCamber\]=&m\[maxThickness\]=&m\[minThickness\]=&m\[grp\]=naca4d&m\[sort\]=1&m\[page\]=2&m\[count\]=30](http://airfoiltools.com/search/index?m[textSearch]=&m[maxCamber]=&m[minCamber]=&m[maxThickness]=&m[minThickness]=&m[grp]=naca4d&m[sort]=1&m[page]=2&m[count]=30) [9 November 2018]

Ahmad K., 2008. CFD Simulation and Wind Tunnel Test of NACA 4412 Airfoil Wing Section at Different Angles of Attack.

Lim, F. K., (2009). *Air Flow Around Bodies In Subsonic Wind Tunnel*.

Çengel, Y. A., & Boles, M. A., 2009. *Thermodynamics: An Engineering Approach*. Boston: McGraw-Hill Higher Education.

(n.d.). Retrieved from https://www.engineeringtoolbox.com/standard-atmosphere-d_604.html [30 October 2018]

Appendix A

Table A.1: Properties of air at 1 atm pressure. (Cengel & Boles, 2015)

948
PROPERTY TABLES AND CHARTS

TABLE A-9
Properties of air at 1 atm pressure

Temp. $T, ^\circ\text{C}$	Density $\rho, \text{kg/m}^3$	Specific Heat c_p $\text{J/kg}\cdot\text{K}$	Thermal Conductivity $k, \text{W/m}\cdot\text{K}$	Thermal Diffusivity $\alpha, \text{m}^2/\text{s}$	Dynamic Viscosity $\mu, \text{kg/m}\cdot\text{s}$	Kinematic Viscosity $\nu, \text{m}^2/\text{s}$	Prandtl Number Pr
-150	2.866	983	0.01171	4.158×10^{-6}	8.636×10^{-6}	3.013×10^{-6}	0.7246
-100	2.038	966	0.01582	8.036×10^{-6}	1.189×10^{-6}	5.837×10^{-6}	0.7263
-50	1.582	999	0.01979	1.252×10^{-5}	1.474×10^{-5}	9.319×10^{-6}	0.7440
-40	1.514	1002	0.02057	1.356×10^{-5}	1.527×10^{-5}	1.008×10^{-5}	0.7436
-30	1.451	1004	0.02134	1.465×10^{-5}	1.579×10^{-5}	1.087×10^{-5}	0.7425
-20	1.394	1005	0.02211	1.578×10^{-5}	1.630×10^{-5}	1.169×10^{-5}	0.7408
-10	1.341	1006	0.02288	1.696×10^{-5}	1.680×10^{-5}	1.252×10^{-5}	0.7387
0	1.292	1006	0.02364	1.818×10^{-5}	1.729×10^{-5}	1.338×10^{-5}	0.7362
5	1.269	1006	0.02401	1.880×10^{-5}	1.754×10^{-5}	1.382×10^{-5}	0.7350
10	1.246	1006	0.02439	1.944×10^{-5}	1.778×10^{-5}	1.426×10^{-5}	0.7336
15	1.225	1007	0.02476	2.009×10^{-5}	1.802×10^{-5}	1.470×10^{-5}	0.7323
20	1.204	1007	0.02514	2.074×10^{-5}	1.825×10^{-5}	1.516×10^{-5}	0.7309
25	1.184	1007	0.02551	2.141×10^{-5}	1.849×10^{-5}	1.562×10^{-5}	0.7296
30	1.164	1007	0.02588	2.208×10^{-5}	1.872×10^{-5}	1.608×10^{-5}	0.7282
35	1.145	1007	0.02625	2.277×10^{-5}	1.895×10^{-5}	1.655×10^{-5}	0.7268
40	1.127	1007	0.02662	2.346×10^{-5}	1.918×10^{-5}	1.702×10^{-5}	0.7255
45	1.109	1007	0.02699	2.416×10^{-5}	1.941×10^{-5}	1.750×10^{-5}	0.7241
50	1.092	1007	0.02735	2.487×10^{-5}	1.963×10^{-5}	1.798×10^{-5}	0.7228
60	1.059	1007	0.02808	2.632×10^{-5}	2.008×10^{-5}	1.896×10^{-5}	0.7202
70	1.028	1007	0.02881	2.780×10^{-5}	2.052×10^{-5}	1.995×10^{-5}	0.7177
80	0.9994	1008	0.02953	2.931×10^{-5}	2.096×10^{-5}	2.097×10^{-5}	0.7154
90	0.9718	1008	0.03024	3.086×10^{-5}	2.139×10^{-5}	2.201×10^{-5}	0.7132
100	0.9458	1009	0.03095	3.243×10^{-5}	2.181×10^{-5}	2.306×10^{-5}	0.7111
120	0.8977	1011	0.03235	3.565×10^{-5}	2.264×10^{-5}	2.522×10^{-5}	0.7073
140	0.8542	1013	0.03374	3.898×10^{-5}	2.345×10^{-5}	2.745×10^{-5}	0.7041
160	0.8148	1016	0.03511	4.241×10^{-5}	2.420×10^{-5}	2.975×10^{-5}	0.7014
180	0.7788	1019	0.03646	4.593×10^{-5}	2.504×10^{-5}	3.212×10^{-5}	0.6992
200	0.7459	1023	0.03779	4.954×10^{-5}	2.577×10^{-5}	3.455×10^{-5}	0.6974
250	0.6746	1033	0.04104	5.890×10^{-5}	2.760×10^{-5}	4.091×10^{-5}	0.6946
300	0.6158	1044	0.04418	6.871×10^{-5}	2.934×10^{-5}	4.765×10^{-5}	0.6935
350	0.5664	1056	0.04721	7.892×10^{-5}	3.101×10^{-5}	5.475×10^{-5}	0.6937
400	0.5243	1069	0.05015	8.951×10^{-5}	3.261×10^{-5}	6.219×10^{-5}	0.6948
450	0.4880	1081	0.05298	1.004×10^{-4}	3.415×10^{-5}	6.997×10^{-5}	0.6965
500	0.4565	1093	0.05572	1.117×10^{-4}	3.563×10^{-5}	7.806×10^{-5}	0.6986
600	0.4042	1115	0.06093	1.352×10^{-4}	3.846×10^{-5}	9.515×10^{-5}	0.7037
700	0.3627	1135	0.06581	1.598×10^{-4}	4.111×10^{-5}	1.133×10^{-4}	0.7092
800	0.3289	1153	0.07037	1.855×10^{-4}	4.362×10^{-5}	1.326×10^{-4}	0.7149
900	0.3008	1169	0.07465	2.122×10^{-4}	4.600×10^{-5}	1.529×10^{-4}	0.7206
1000	0.2772	1184	0.07868	2.398×10^{-4}	4.826×10^{-5}	1.741×10^{-4}	0.7260
1500	0.1990	1234	0.09599	3.908×10^{-4}	5.817×10^{-5}	2.922×10^{-4}	0.7478
2000	0.1553	1264	0.11113	5.664×10^{-4}	6.630×10^{-5}	4.270×10^{-4}	0.7539

Note: For ideal gases, the properties c_p , k , μ , and Pr are independent of pressure. The properties ρ , ν , and α at a pressure P (in atm) other than 1 atm are determined by multiplying the values of ρ at the given temperature by P and by dividing ν and α by P .

Source: Data generated from the EES software developed by S. A. Klein and F. L. Alvarado. Original sources: Keenan, Chao, Keyes, Gas Tables, Wiley, 198; and Thermophysical Properties of Matter, Vol. 3: Thermal Conductivity, Y. S. Touloukian, P. E. Liley, S. C. Saxena, Vol. 11: Viscosity, Y. S. Touloukian, S. C. Saxena, and P. Hestermans, IFI/Plenum, NY, 1970, ISBN 0-306067020-8.

Appendix B

Table B.1: US Standard Atmosphere Air Properties – SI Units (Source:

https://www.engineeringtoolbox.com/standard-atmosphere-d_604.html)

Geo potential Altitude above Sea Level - h - (m)	Temperature - t - (°C)	Acceleration of Gravity - g - (m/s ²)	Absolute Pressure - p - (10 ⁴ N/m ²)	Density - ρ - (kg/m ³)	Dynamic Viscosity - μ - (10 ⁻⁵ N s/m ²)
-1000	21.50	9.810	11.39	1.347	1.821
0	15.00	9.807	10.13	1.225	1.789
1000	8.50	9.804	8.988	1.112	1.758
2000	2.00	9.801	7.950	1.007	1.726
3000	-4.49	9.797	7.012	0.9093	1.694
4000	-10.98	9.794	6.166	0.8194	1.661
5000	-17.47	9.791	5.405	0.7364	1.628
6000	-23.96	9.788	4.722	0.6601	1.595
7000	-30.45	9.785	4.111	0.5900	1.561
8000	-36.94	9.782	3.565	0.5258	1.527
9000	-43.42	9.779	3.080	0.4671	1.493
10000	-49.90	9.776	2.650	0.4135	1.458
15000	-56.50	9.761	1.211	0.1948	1.422
20000	-56.50	9.745	0.5529	0.08891	1.422
25000	-51.60	9.730	0.2549	0.04008	1.448
30000	-46.64	9.715	0.1197	0.01841	1.475
40000	-22.80	9.684	0.0287	0.003996	1.601
50000	-2.5	9.654	0.007978	0.001027	1.704
60000	-26.13	9.624	0.002196	0.0003097	1.584
70000	-53.57	9.594	0.00052	0.00008283	1.438
80000	-74.51	9.564	0.00011	0.00001846	1.321

Take Jabiru J200 wing as the model for the kinematic similarity.

Specification for Jabiru J200:

Airfoil Type: NACA 4412

Wing Span: 8.100 m

Wing Area: 8.083 m²

Cruise Speed: 120 kts @ 61.73 m/s

Wing Area = Chord Length x Wingspan

$$\text{Thus, Chord Length, } L_c = \frac{\text{Wing Area}}{\text{Wing Span}}$$

$$= \frac{8.083}{8.100}$$

$$= 0.9979$$

$\approx 1 \text{ m}$

Assume that the Jabiru J200 airplane at 1500m above the sea level,

Referring to Table B.1 , the temperature, density and dynamic viscosity of the air at different altitude are obtained by doing linear interpolation as shown in Table B.2.

Table B.2: Linear interpolation.

Altitude, h (m)	Temperature, T (°C)	Density, ρ_p (kg/m ³)	Dynamic Viscosity, μ_p (Ns/m ²)
1000	8.5	1.112	1.758
1500	x	y	z
2000	2.0	1.007	1.726

For temperature,

$$\frac{1500 - 1000}{2000 - 1000} = \frac{x - 8.5}{2.0 - 8.5}$$

$$x = 5.25^\circ\text{C}$$

For density,

$$\frac{1500 - 1000}{2000 - 1000} = \frac{y - 1.112}{1.007 - 1.112}$$

$$y = 1.06 \text{ kg/m}^3$$

For dynamic viscosity,

$$\frac{1500 - 1000}{2000 - 1000} = \frac{y - 1.758}{1.726 - 1.758}$$

$$z = 1.742 \times 10^{-5} \text{ Ns/m}^2 @ \text{ kg/ms}$$

Assume the air in FKM's subsonic wind tunnel is at 25 °C and 1 atm and take this as the air for the model. By using Cengel's properties of air at 1 atm table in Appendix A.

At 25 °C,

the air density, $\rho_m = 1.184 \text{ kg/m}^3$ and the dynamic viscosity, $\mu_m = 1.849 \times 10^{-5} \text{ kg/ms}$.

The maximum air velocity for the subsonic wind tunnel is 30 m/s.

Kinematic similarity using Reynolds number from eq (2.12)

$$Re_p = Re_m$$

$$\left(\frac{\rho V L c}{\mu}\right)_p = \left(\frac{\rho V L c}{\mu}\right)_m$$

$$L_{cm} = (L_{cp}) (\rho_p/\rho_m) (V_p/V_m) (\mu_p/\mu_m)$$

$$= (1\text{m}) \left(\frac{1.06}{1.184}\right) \left(\frac{61.73}{30}\right) \left(\frac{1.849 \times 10^{-5}}{1.184 \times 10^{-5}}\right)$$

$$= 2.88 \text{ m}$$

The calculated chord length, L_c for the airfoil model longer than the test section in FKM's subsonic wind tunnel and it is unable to be fabricated in prototype lab. Thus, an airfoil model of 100 mm in chord length and 100 mm width is used for the experiment in wind tunnel since an NACA 0015 model with the same dimension given to the Turbomachinery lab by the company that make the wind tunnel.

Appendix C

Table C1: Gantt chart for PSM I

Week Activities	1	2	3	4	5	6	7	8	9	10	11	12	13	14	15	16
Find supervisor																
Project title confirmation										M I D S E M						
Discussion with supervisor										B R E A K						
Research study																
Writing report																
Introduction																
Submission of progress report 1																
Literature review																
Methodology																
Slide presentation with supervisor																
Submission of final report																
PSM 1 presentation																

Table C2: Gantt chart for PSM II

Week \ Activities	1	2	3	4	5	6	7	8	9	10	11	12	13	14	15
Simulation of Airfoils															
Data collection										M					
Data analyze										I					
Submission of progress report 2										D					
Report writing										S					
Submission of report										E					
PSM 2 presentation										M					
										B					
										R					
										E					
										A					
										K					



Appendix D

NACA 4412 –Results using S-A Model

Table D.1: Results for NACA 4412 at 10 m/s using S-A Model

NACA 4412 (10 m/s)				
Angle of Attack	Force		Coefficient	
	Lift	Drag	Lift	Drag
0	0.07722	0.02208	0.01304322	0.00373
5	0.19607	0.03579	0.03311969	0.00605
10	0.30746	0.06043	0.0519366	0.01021
15	0.40995	0.09892	0.06924841	0.01671
20	0.51629	0.15371	0.08721143	0.02596
25	0.60943	0.22182	0.10294407	0.03747
30	0.67833	0.32718	0.11458295	0.05527
35	0.72875	0.4384	0.12309968	0.07405
40	0.74947	0.5418	0.12659917	0.09152
45	0.70985	0.62677	0.11990695	0.10587
50	0.63228	0.66462	0.10680382	0.11227

Table D.2: Results for NACA 4412 at 20 m/s using S-A Model

NACA 4412 (20 m/s)				
Angle of Attack	Force		Coefficient	
	Lift	Drag	Lift	Drag
0	0.33782	0.08211	0.01426588	0.00347
5	0.72767	0.13568	0.03072942	0.00573
10	1.13022	0.23462	0.04772881	0.00991
15	1.47255	0.42321	0.06218527	0.01787
20	1.75421	0.71244	0.07407966	0.03009
25	1.99091	1.02997	0.08407571	0.0435
30	2.19562	1.38733	0.09272026	0.05859
35	2.35085	1.77224	0.09927584	0.07484
40	2.47329	2.1238	0.10444632	0.08969
45	2.51349	2.39441	0.10614393	0.10112
50	2.39593	2.6984	0.1011793	0.11395

Table D.3: Results for NACA 4412 at 30 m/s using S-A Model

NACA 4412 (30 m/s)				
Angle of Attack	Force		Coefficient	
	Lift	Drag	Lift	Drag
0	0.74167	0.17733	0.01392	0.00333
5	1.6555	0.29849	0.03107	0.0056
10	2.45179	0.62187	0.04602	0.01167
15	3.18285	1.1305	0.05974	0.02122
20	3.73783	1.67676	0.07015	0.03147
25	4.25012	2.39988	0.07977	0.04504
30	4.79573	3.2606	0.09001	0.0612
35	5.18971	4.08188	0.0974	0.07661
40	5.63054	4.78308	0.10568	0.08977
45	5.76731	5.3841	0.10825	0.10105
50	5.37634	6.06512	0.10091	0.11383

NACA 4412 –Results using SST Model

Table D.4: Results for NACA 4412 at 10 m/s using SST Model

NACA 4412 (10 m/s)				
Angle of attack	Force		Coefficient	
	Lift	Drag	Lift	Drag
0	0.07446	0.02086	0.01258	0.00352
5	0.18181	0.03224	0.03071	0.00545
10	0.28734	0.05571	0.04854	0.00941
15	0.39311	0.0915	0.0664	0.01546
20	0.48916	0.14327	0.08263	0.0242
25	0.58353	0.2141	0.09857	0.03617
30	0.65635	0.32011	0.11087	0.05407
35	0.71243	0.42384	0.12034	0.0716
40	0.73452	0.52913	0.12407	0.08938
45	0.69413	0.6083	0.11725	0.10275
50	0.61705	0.65037	0.10423	0.10986

Table D.5: Results for NACA 4412 at 20 m/s using SST Model

NACA 4412 (20 m/s)				
Angle of attack	Force		Coefficient	
	Lift	Drag	Lift	Drag
0	0.31832	0.07542	0.01344	0.00319
5	0.69197	0.12395	0.02922	0.00523
10	1.03798	0.21868	0.04383	0.00923
15	1.35525	0.37055	0.05723	0.01565
20	1.6187	0.62083	0.06836	0.02622
25	1.8387	0.9387	0.07765	0.03964
30	2.03652	1.27827	0.086	0.05398
35	2.19034	1.6102	0.0925	0.068
40	2.32822	1.97613	0.09832	0.08345
45	2.35573	2.26972	0.09948	0.09585
50	2.23683	2.55643	0.09446	0.10796

Table D.6: Results for NACA 4412 at 30 m/s using SST Model

NACA 4412 (30 m/s)				
Angle of attack	Force		Coefficient	
	Lift	Drag	Lift	Drag
0	0.74167	0.17733	0.01392	0.00333
5	1.54563	0.29506	0.02901	0.00554
10	2.24246	0.51827	0.04209	0.00973
15	2.93003	0.87222	0.05499	0.01637
20	3.53144	1.36763	0.06628	0.02567
25	4.0366	2.09339	0.07576	0.03929
30	4.53961	2.87546	0.0852	0.05397
35	4.92734	3.67685	0.09248	0.06901
40	5.19626	4.37238	0.09753	0.08206
45	5.28988	5.10088	0.09928	0.09574
50	5.01922	5.73973	0.0942	0.10773

Appendix E

NACA 4418 –Results using S-A Model

Table E.1: Results for NACA 4418 at 10 m/s using S-A Model

NACA 4418 (10 m/s)				
Angle of Attack	Force		Coefficient	
	Lift	Drag	Lift	Drag
0	0.07302	0.03092	0.01233	0.00522
5	0.20733	0.05158	0.03502	0.00871
10	0.33227	0.08059	0.05613	0.01361
15	0.44242	0.11739	0.07473	0.01983
20	0.53648	0.1661	0.09062	0.02806
25	0.63631	0.2412	0.10749	0.04074
30	0.72466	0.3459	0.12241	0.05843
35	0.79878	0.47594	0.13493	0.0804
40	0.85164	0.57659	0.14386	0.0974
45	0.81987	0.67328	0.13849	0.11373
50	0.73244	0.75329	0.12372	0.12725

Table E.2: Results for NACA 4418 at 20 m/s using S-A Model

NACA 4418 (20 m/s)				
Angle of Attack	Force		Coefficient	
	Lift	Drag	Lift	Drag
0	0.31854	0.09952	0.01345	0.0042
5	0.70723	0.13985	0.02987	0.00591
10	1.16728	0.29381	0.04929	0.01241
15	1.56043	0.45017	0.0659	0.01901
20	1.90124	0.72516	0.08029	0.03062
25	2.14387	1.08478	0.09053	0.04581
30	2.39331	1.43571	0.10107	0.06063
35	2.59622	1.79571	0.10964	0.07583
40	2.76549	2.16441	0.11679	0.0914
45	2.84153	2.50534	0.12	0.1058
50	2.71409	2.83256	0.11462	0.11962

Table E.3: Results for NACA 4418 at 30 m/s using S-A Model

NACA 4418 (30 m/s)				
Angle of Attack	Force		Coefficient	
	Lift	Drag	Lift	Drag
0	0.75191	0.23013	0.01411	0.00432
5	1.64026	0.508	0.03079	0.00953
10	2.61931	0.77222	0.04916	0.01449
15	3.42006	1.1519	0.06419	0.02162
20	4.13844	1.61959	0.07767	0.0304
25	4.6938	2.37497	0.0881	0.04458
30	5.29546	3.24256	0.09939	0.06086
35	5.79487	4.11326	0.10876	0.0772
40	6.2585	4.86364	0.11746	0.09128
45	6.5332	5.64288	0.12262	0.10591
50	6.14757	6.32125	0.11538	0.11864

NACA 4418 –Results using SST Model

Table E.4: Results for NACA 4418 at 10 m/s using SST Model

NACA 4418 (10 m/s)				
Angle of attack	Force		Coefficient	
	Lift	Drag	Lift	Drag
0	0.07213	0.02946	0.01218	0.00498
5	0.19438	0.04863	0.03283	0.00821
10	0.30569	0.07288	0.05164	0.01231
15	0.41352	0.10078	0.06985	0.01702
20	0.51371	0.15233	0.08678	0.02573
25	0.61561	0.22752	0.10399	0.03843
30	0.69815	0.32966	0.11793	0.05569
35	0.77792	0.45068	0.13141	0.07613
40	0.83699	0.55892	0.14138	0.09441
45	0.80158	0.64172	0.1354	0.1084
50	0.68057	0.70434	0.11496	0.11898

Table E.5: Results for NACA 4418 at 20 m/s using SST Model

NACA 4418 (20 m/s)				
Angle of attack	Force		Coefficient	
	Lift	Drag	Lift	Drag
0	0.30689	0.09875	0.01296	0.00417
5	0.75821	0.13863	0.03202	0.00585
10	1.13485	0.25384	0.04792	0.01072
15	1.48582	0.43195	0.06275	0.01824
20	1.78754	0.67756	0.07549	0.02861
25	2.03758	1.02509	0.08605	0.04329
30	2.2797	1.37627	0.09627	0.05812
35	2.52643	1.73079	0.10669	0.07309
40	2.69117	2.06308	0.11365	0.08712
45	2.7468	2.37673	0.116	0.10037
50	2.62113	2.7277	0.11069	0.11519

Table E.6: Results for NACA 4418 at 30 m/s using SST Model

NACA 4418 (30 m/s)				
Angle of attack	Force		Coefficient	
	Lift	Drag	Lift	Drag
0	0.74992	0.22718	0.01408	0.00426
5	1.63074	0.44735	0.03061	0.0084
10	2.59644	0.71541	0.04873	0.01343
15	3.37258	1.01221	0.0633	0.019
20	4.02386	1.52042	0.07552	0.02854
25	4.57922	2.26019	0.08595	0.04242
30	5.06236	3.12032	0.09501	0.05856
35	5.51425	3.9434	0.1035	0.07401
40	5.93429	4.61089	0.11138	0.08654
45	6.17942	5.32445	0.11598	0.09993
50	5.91974	6.14914	0.11111	0.11541